

Structure Detection for Contextual Reinforcement Learning

Tianyue Zhou*, Jung-Hoon Cho*, Cathy Wu

Massachusetts Institute of Technology
 {tianyuez, jhooncho, cathywu}@mit.edu

Abstract

Contextual Reinforcement Learning (CRL) tackles the problem of solving a set of related Contextual Markov Decision Processes (CMDPs) that vary across different context variables. Traditional approaches—*independent training* and *multi-task learning*—struggle with either excessive computational costs or negative transfer. A recently proposed multi-policy approach, Model-Based Transfer Learning (MBTL), has demonstrated effectiveness by strategically selecting a few tasks to train and zero-shot transfer. However, CMDPs encompass a wide range of problems, exhibiting structural properties that vary from problem to problem. As such, different task selection strategies are suitable for different CMDPs. In this work, we introduce Structure Detection MBTL (SD-MBTL), a generic framework that dynamically identifies the underlying generalization structure of CMDP and selects an appropriate MBTL algorithm. For instance, we observe MOUNTAIN structure in which generalization performance degrades from the training performance of the target task as the context difference increases. We thus propose M/GP-MBTL, which detects the structure and adaptively switches between a Gaussian Process-based approach and a clustering-based approach. Extensive experiments on synthetic data and CRL benchmarks—covering continuous control, traffic control, and agricultural management—show that M/GP-MBTL surpasses the strongest prior method by 12.49% on the aggregated metric. These results highlight the promise of online structure detection for guiding source task selection in complex CRL environments.

Code — <https://github.com/mit-wu-lab/SD-MBTL/>
Webpage — <https://mit-wu-lab.github.io/SD-MBTL/>

1 Introduction

Despite the recent success of deep reinforcement learning (RL), deep RL often struggles to solve real-world applications that involve families of related tasks that differ in a few key parameters but mostly share underlying dynamics (Bellemare et al. 2020; Degrave et al. 2022; Benjamins et al. 2023). Such contextual variations naturally arise in robotics (e.g., different payload weights or terrain conditions) (Yu et al. 2020) and traffic control (e.g., varying traffic inflows or signal timing) (Jayawardana et al. 2025). Formally, these settings

can be modeled as Contextual Markov Decision Processes (CMDPs) (Hallak, Di Castro, and Mannor 2015; Modi et al. 2018; Benjamins et al. 2023), where each task is specified by a context. Moreover, we extend prior studies to more challenging multi-dimensional CMDP, rather than a single-dimensional context.

Due to the curse of dimensionality in context variables, a central challenge in CMDPs is how to efficiently train policies that generalize to numerous related tasks without starting training from scratch. Existing paradigms for CMDPs include: (1) Independent training of a separate policy for each task, which is straightforward but computationally expensive for large task families; (2) Multi-task training of a single universal policy conditioned on the context, which can suffer from limited model capacity or negative transfer if tasks are too dissimilar (Kang, Grauman, and Sha 2011; Standley et al. 2020); and (3) Multi-policy training on a small subset of source tasks *with zero-shot transfer* to new tasks, raising the key question of how to choose that subset. Recent work has shown that carefully selecting which tasks to train on can lead to strong generalization and improved sample efficiency (Cho et al. 2023, 2024), since the cost of full training far outweighs the cost of policy evaluation and the task-selection.

Multi-policy training requires selecting a subset of tasks in CMDPs, formulated as a Greedy Tasks Selection Problem (GSTS). However, many CMDPs exhibit specific structural patterns that can be exploited. For example, (Cho et al. 2024) splits generalization performance into training performance and a generalization gap, modeling the gap as a linear function. Inspired by this, we define a task structure as a functional decomposition of generalization performance in which certain components satisfy designated properties. We thus propose a generic *Structure Detection Model-Based Transfer Learning* (SD-MBTL) framework, which detects the underlying structure and adapts its task selection strategy accordingly. In this paper, we instantiate the SD-MBTL framework with **M/GP-MBTL**, which uses two specific structures and dynamically switches between task selection algorithms—Gaussian Process-based and clustering-based MBTL (Figure 1).

For example, we observe experimentally that generalization in CMDPs often follow some structure, in which we find some task selection approach works better. Thus, detecting such structure enables a more targeted approach to source task selection than a one-size-fits-all approach. To capitalize

*These authors contributed equally.

Copyright © 2026, Association for the Advancement of Artificial Intelligence (www.aaai.org). All rights reserved.

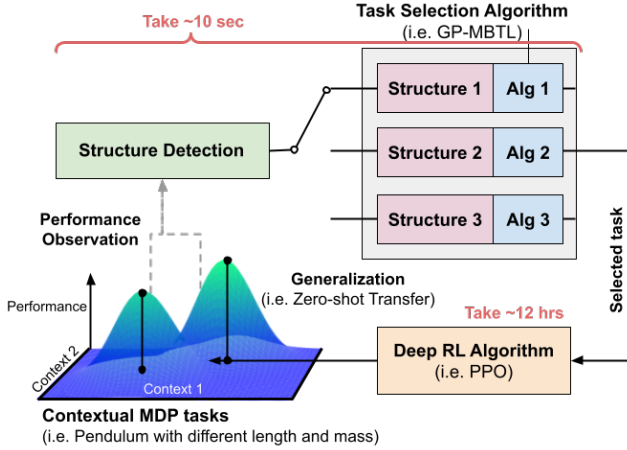


Figure 1: **Conceptual overview.** SD-MBTL detects an underlying structure from observed generalization performance and selects an appropriate algorithm.

on this insight, we also devise a fast and effective algorithm, MOUNTAIN Model-Based Transfer Learning (M-MBTL), by reducing GSTS problem to a sequential version of clustering problem upon a certain MOUNTAIN structure. It enables us to leverage clustering loss to efficiently guide the search of the training task in a continuous space.

Our main contributions are summarized as follows:

- We introduce SD-MBTL, a unified framework that detects the underlying generalization structure of CMDPs and adapts its source-task selection strategy, resulting in improved sample efficiency in diverse CRL settings.
- We propose M/GP-MBTL, a practical structure detection algorithm, using two specific structures in the generalization performance. We also develop a clustering-based MBLT algorithm for MOUNTAIN structure.
- We empirically validate our approach in a multi-dimensional synthesized dataset and real-world CMDP benchmarks, including continuous control (CartPole and BipedalWalker (Benjamins et al. 2023)), cooperative eco-driving (IntersectionZoo (Jayawardana et al. 2025)), and crop management (CyclesGym (Turchetta et al. 2022)). On the aggregated metric normalized between the random baseline and the oracle, M/GP-MBTL outperforms the previous best method by 12.49%.

The rest of the article is structured as follows: Section 2 reviews CMDP and GSTS problem. Section 3 introduces the SD-MBTL framework. Section 4 introduces M/GP-MBTL. Section 5 presents evaluations on benchmarks, Section 6 discusses related work, and Section 7 concludes.

2 Preliminaries

2.1 Contextual Markov Decision Process

We consider a *contextual* Markov decision process (CMDP) defined over a family of MDPs indexed by a *context* (or *task*) variable in a multi-dimensional space. Let the finite set of all MDPs (or tasks) be denoted by $Y = \{y_1, y_2, \dots, y_N\}$, where

each task $y_n \in \mathbb{R}^D$ for some dimension D , and $N = |Y|$ is the total number of tasks (or target tasks). Specifically, let each task $y \in Y \subset \mathbb{R}^D$ parameterize a distinct MDP $\mathcal{M}_y = (S, A, P_y, R_y, \rho_y)$, where S is the state space, A is the action space, P_y represents transition dynamics, R_y is the reward function, and ρ_y is the initial state distribution for the task y (Hallak, Di Castro, and Mannor 2015; Modi et al. 2018). Hence, the CMDP is the collection $\{\mathcal{M}_y\}_{y \in Y}$.

We define a continuous set of tasks $X \subset \mathbb{R}^D$ such that X has the same bound as Y . Intuitively, X captures an underlying continuous space of tasks from which Y can be viewed as a discrete subset ($Y \subset X$). Given a context $x \in X$, one can train a policy π_x (using, for instance, an off-the-shelf RL algorithm) and get the (*source*) *training performance* on task x by $J(\pi_x, x) = \mathbb{E}[\text{return of } \pi_x \text{ in } \mathcal{M}_x]$. To zero-shot transfer from a source task x to a target task y , we apply the policy π_x (trained on \mathcal{M}_x) within \mathcal{M}_y , potentially at reduced performance compared to training directly on y . The resulting *generalization performance* is $J(\pi_x, y)$. We quantify the zero-shot generalization gap when transferring from x to y as $\Delta J(\pi_x, y) = J(\pi_x, x) - J(\pi_x, y)$.

2.2 Problem Formulation

Greedy source task selection (GSTS) problem¹ Given a CMDP with a finite set of *target tasks* Y , our goal is to identify a sequence of tasks on which to perform full RL training, so as to achieve high generalization performance on all tasks in Y . Specifically, at each step k , we pick a new source task $x_k \in X$ to train a corresponding policy π_{x_k} . For each task in Y , we choose the best performing policy from a set of trained policies, which maximizes the performance. The objective at each round k is to *greedily* select a new source task x_k that maximizes the expected performance across the entire set Y . One can write this as:

$$x_k = \arg \max_{x \in X \setminus \{x_{1:k-1}\}} \mathbb{E}_{y \sim \mathcal{U}(Y)} \left[\max_{x' \in x_{1:k-1} \cup \{x\}} J(\pi_{x'}, y) \right] \quad (1)$$

where $x_{1:K} = x_1, \dots, x_K$, and $\mathcal{U}(Y)$ is a uniform distribution over the finite task set Y . In general, an exact solution to GSTS problems can be intractable for large-scale or continuous task spaces. In practice, many applications have fairly small task spaces (e.g., 3-10 context dimensions, each discretized to 100 values). The core challenge is that solving *any* task MDP is fairly expensive and thus the number of task MDPs to solve should be minimized. MBLT aimed to circumvent naive exploration by modeling the training performance and generalization gap and optimizing the selection via Bayesian optimization (Cho et al. 2024).

2.3 Model-Based Transfer Learning

A practical solution to solve GSTS problem is provided by MBLT (Cho et al. 2024), which we refer to as **GP-MBTL** in this work. GP-MBTL discretizes the continuous source-task

¹This was defined as the Sequential Source Task Selection problem in (Cho et al. 2024). We renamed the problem because its goal is to greedily select a training task at each step, and the term “sequential” fails to convey this aspect.

space, models source-task returns with Gaussian-Process regression, and approximates the generalization gap as a linear function of context similarity. At each iteration k , it selects the source task x_k that maximizes an acquisition function combining predicted source task performance $\mu_{k-1}(x)$, uncertainty $\sigma_{k-1}(x)$, and the estimated generalization gap to target tasks. The policy trained on x_k is then evaluated, and the GP posterior updated, progressively improving coverage of the target set Y . We additionally use observed transfer performance to refine the acquisition rule and estimate the gap’s slope online. Full derivations, algorithmic details, and hyperparameters are provided in Appendix I.

3 Structure Detection Model-Based Transfer Learning

CMDPs with multi-dimensional context spaces typically demand significantly more data to keep model predictions accurate, which challenges the Gaussian-process module in GP-MBTL and complicates the exploration-exploitation trade-off. When a CMDP obeys a recognisable structure, however, that structure can be detected and then exploited to curb unnecessary exploration. We therefore introduce a generic **Structure Detection Model-Based Transfer Learning** (SD-MBTL) framework for task selection.

3.1 Generalization Performance Structure Decomposition

To support the identification and analysis of CMDP structures, we decompose the generalization-performance structure inspired by the Sobol-Hoeffding (functional-ANOVA) decomposition, which uniquely and orthogonally splits any square-integrable multivariate function into additive main-effect terms and interaction terms (Hoeffding 1948; Sobol’ 1990). More details on how we derive this decomposition are provided in Appendix C.

Definition 3.1 (Generalization Performance Structure Decomposition). For any task pair (x, y) , define $C := \mathbb{E}_{x \in X, y \in Y} [J(\pi_x, y)]$, $g(y) := \mathbb{E}_{x \in X} [J(\pi_x, y)] - C$, $f(x) := J(\pi_x, x) - g(x) - C$, and $h(x, y) := J(\pi_x, y) - f(x) - g(y) - C$, thus we can get:

$$J(\pi_x, y) = f(x) + g(y) + h(x, y) + C, \quad (2)$$

and $h(x, y) = 0$ if $x = y$.

Based on empirical observations, we found three components that affect generalization performance: 1) The intrinsic quality of source policy influences whether it has good generalization across many tasks. 2) The difficulty of the target task affects whether transferred policies can achieve high performance on it. 3) The dissimilarity between source and target tasks degrades generalization performance, as large differences in context usually yield poor generalization. Thus, we name $f(x)$ as the **policy quality**, $g(y)$ as the **task difficulty**, and $h(x, y)$ as the **task dissimilarity** between source and target tasks.

Based on the decomposition, we outline the procedure for addressing a CMDP by exploiting a specific structure. Within a CMDP structure, one or more of $f(x)$, $g(y)$, and $h(x, y)$

may satisfy particular assumptions or properties, allowing us to treat them as known components of $J(\pi_x, y)$. Thus, a corresponding algorithm can be used to learn the remaining unknown components and select training tasks based on the model so as to maximize the objective.

3.2 SD-MBTL

SD-MBTL embeds a dynamic structure detection mechanism inside the MBTL loop and chooses the corresponding MBTL algorithm based on the detected structure. Its inputs are (i) a set of candidate CMDP structures \mathcal{S} , (ii) a detection routine $\text{Detect} : \mathbb{R}^{k \times N} \rightarrow \mathcal{S}$, and (iii) a library of MBTL algorithms $\{\text{Alg}_1, \dots, \text{Alg}_{|\mathcal{S}|}\}$ matched one-to-one with the structures in \mathcal{S} . At each decision round, SD-MBTL uses the observed generalization performances $\{J(\pi_{x_\kappa}, y_n)\}_{n \in [N], \kappa \in [k]}$ to infer the current structure $s_i = \text{Detect}(\cdot)$, then invokes the corresponding algorithm Alg_i to choose the next training task x . After training, the new policy π_x is transferred to all target tasks, yielding zero-shot generalization performances $\{J(\pi_x, y_n)\}_{n \in [N]}$. More details in SD-MBTL are provided in Appendix K.

4 M/GP Model-Based Transfer Learning

As a concrete instantiation of SD-MBTL, we propose **M/GP-MBTL**, which targets a special CMDP structure—**MOUNTAIN**. When the CMDP satisfies MOUNTAIN, the GSTS problem reduces to clustering, and we employ the clustering-based M-MBTL. Otherwise, we revert to the more general GP-MBTL. This two-way strategy combines the sample efficiency of M-MBTL with the robustness of GP-MBTL.

4.1 MOUNTAIN Structure

In our experiments, we observe that some CMDP problems exhibit similar model structures. Figure 2 shows the policy quality $f(x)$, task difficulty $g(y)$, and task dissimilarity $h(x, y)$ in CartPole, BipedalWalker, and CyclesGym benchmarks. In these tasks, $f(x)$ is nearly constant. $h(x, y)$ decreases approximately linearly as the context difference increases, resembling a distance metric. These similar characteristics suggest that they may originate from the same underlying structure. Thus, we identify a specific generalization structure—termed **MOUNTAIN** structure—that relies on the following key assumptions.

Assumption 4.1 (Constant Source Task Influence). Policy quality is constant: $f(x) = C_1$.

Assumption 4.2 (Distance Metric for Task Dissimilarity). The task dissimilarity $h(x, y)$ is represented as a distance metric: $h(x, y) = -\text{dist}(x, y)$. The distance metric (Čech and Katětov 1969) is a function $\text{dist} : \mathbb{R}^D \times \mathbb{R}^D \rightarrow \mathbb{R}$ which satisfies $\text{dist}(x, x) = 0 \ \forall x$, positivity, symmetry, and the triangle inequality. In this paper, we use the L_1 norm as the distance metric for our algorithms.

The linear generalization gap assumption in (Cho et al. 2023) and (Cho et al. 2024) assumes $J(\pi_x, y) - J(\pi_x, x) = g(y) - g(x) + h(x, y) = k|x - y|$. It can be considered a specific case of Assumption 4.2, where the CMDP is one-dimensional and target task difficulties $g(y)$ are constant.

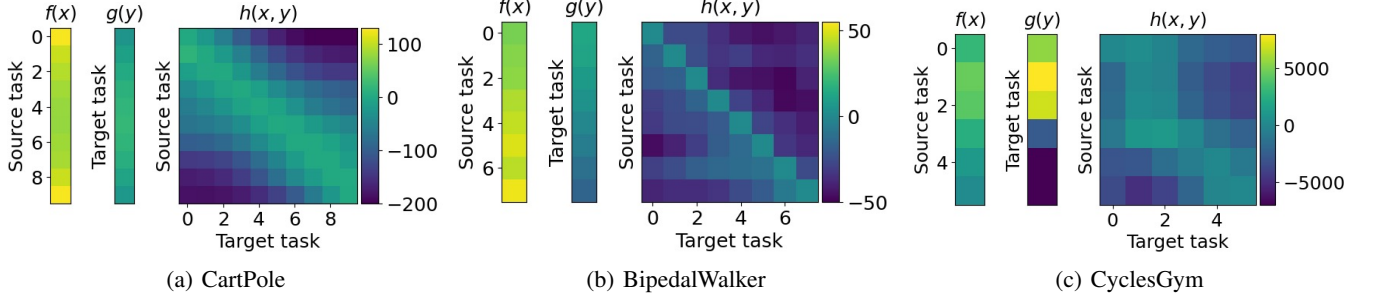


Figure 2: Heatmap of policy quality $f(x)$, task difficulty $g(y)$, and task dissimilarity $h(x, y)$ for CartPole (mass of cart), BipedalWalker (scale), and CyclesGym (precipitation) averaged over three different random seeds. In these tasks, $f(x)$ is nearly constant. $h(x, y)$ decreases approximately linearly as the context difference increases, resembling a distance metric.

Definition 4.3 (MOUNTAIN Structure). MOUNTAIN is a CMDP structure where Assumption 4.1 and 4.2 holds. Or equivalently, $J(\pi_x, y) = J(\pi_y, y) - \text{dist}(x, y)$.

The proof of equivalence is provided in Appendix D. We refer to this as MOUNTAIN because the training performance of the target task resembles mountain peaks, and the generalization performance acts like a slope that decreases as the distance between source and target tasks increases. This perspective effectively reduces GSTS to a clustering problem, which will be discussed in Section 4.3.

4.2 Structure Detection

For an unknown CMDP, we aim to determine whether it satisfies MOUNTAIN structure. At each step k we have observed the generalization performances $J(\pi_x, y)$ for all $x \in \{x_1, \dots, x_k\}$. Our goal is to test whether $f(x)$ and $\text{dist}(x, y)$ individually obey Assumptions 4.1 and 4.2. Because MOUNTAIN structure does not include an explicit task difficulty term $g(y)$, we first remove the influence of task difficulty on $J(\pi_x, y)$ when performing structure detection. Then we apply two criteria: (i) a Small Variance Criterion to check whether policy quality is almost constant (Assumption 4.1), and (ii) a Slope Criterion to check that the majority of slopes are decreasing like a distance metric (Assumption 4.2). If both criteria are satisfied, we tag the CMDP as MOUNTAIN.

Removing the influence of task difficulty. For each step k , we estimate the difficulty of target task by the mean generalization performance of trained policies.

$$g(y) \approx \mathbb{E}_{x \in x_{1:k}}[J(\pi_x, y)] - C. \quad (3)$$

This estimate replaces $x \in X$ in the Definition 3.1 with $x \in x_{1:k}$, because at step k we only have access to the information in $x_{1:k}$. For any training task set $x_{1:k}$ at step k , we define the relative generalization performance as the difference between real generalization performance and its expectation over training tasks: $\bar{J}(\pi_x, y) := J(\pi_x, y) - \mathbb{E}_{x' \in x_{1:k}}[J(\pi_{x'}, y)]$. By removing the influence of task difficulty $g(y)$ by Equation 3, we can have $\bar{J}(\pi_x, y) \approx f(x) + h(x, y)$.

Small Variance Criterion. Although Assumption 4.1 treats policy quality $f(x)$ as a constant, a small variance in $f(x)$ does not materially distort the structure. We therefore

compare the standard deviations of $f(x)$ with task dissimilarity $h(x, y)$ to verify that $f(x)$ indeed exhibits small deviation.

Lemma 4.4 (Relative Influence of Policy Quality and Task Dissimilarity). If $\text{std}_{x \in x_{1:k}}(\bar{J}(\pi_x, x)) < \mathbb{E}_{x \in x_{1:k}}[\text{std}_{y \in Y}(\bar{J}(\pi_x, y))]$, then we have $\text{std}_{x \in x_{1:k}}(f(x)) < \mathbb{E}_{x \in x_{1:k}}[\text{std}_{y \in Y}(h(x, y))]$.

When Lemma 4.4 holds, policy quality $f(x)$ has a relatively small variance. The proof is provided in Appendix E. Define $\mathbb{I}(\cdot)$ as the indicator function. Thus, for any training task set $x_{1:k}$ at step k , we have the following criterion:

Small Variance Criterion

$$:= \mathbb{I}(\text{std}_{x \in x_{1:k}}(\bar{J}(\pi_x, x)) < \mathbb{E}_{x \in x_{1:k}}[\text{std}_{y \in Y}(\bar{J}(\pi_x, y))]). \quad (4)$$

Slope Criterion. A distance metric $\text{dist}(x, y)$ shows both downward slopes on both sides of the source task, while Assumption 4.2 can be violated by the case where $h(x, y)$ have different slope signs. To capture this, we regress the observed generalization performance on signed context differences and extract the left- and right-hand slope vectors $\theta_L, \theta_R \in \mathbb{R}^D$. We verify this structure by checking whether the majority of slopes are indeed decreasing, which is equivalent to confirming that the slope signs on both sides are the same, excluding cases where both sides slope upward. Thus, we have:

$$\text{Slope criterion} := \mathbb{I}\left(\frac{1}{D} \sum_{d=1}^D \mathbb{I}[\text{sgn}(\theta_L^d) = \text{sgn}(\theta_R^d)] > \frac{1}{2}\right), \quad (5)$$

where θ_L^d and θ_R^d represents the slope in the d -th dimension. More details are provided in Appendix G. We define $\text{Detect}(\{J(\pi_\kappa, y_n)\}_{n \in [N], \kappa \in [k-1]}) = \text{MOUNTAIN}$ if both criteria are satisfied; otherwise, the result is NONE.

4.3 MOUNTAIN Model-Based Transfer Learning

Under MOUNTAIN, GSTS problem is reduced to a sequential clustering problem (Lemma 4.5). Proof is provided in Appendix F. Specifically, the reduced problem is a sequential minimization of the total distance between target tasks and their corresponding source tasks. Thus, a clustering loss function can be used to search for training tasks fast and accurately in a continuous set X .

Lemma 4.5 (Reduction of GSTS to Clustering). *With the MOUNTAIN structure, GSTS problem reduces to the sequential version of the clustering problem. Thus, a clustering loss function can be used to search for training tasks fast and accurately in a continuous set X .*

$$\text{for } k \in [K] : x_k = \arg \min_x \mathbb{E}_{y_n} [\min_{x' \in x_{1:k-1} \cup \{x\}} \text{dist}(x', y_n)] \quad (6)$$

Our MOUNTAIN Model-Based Transfer Learning (M-MBTL) extends K-Means to this sequential setting. Because fixing earlier centroids can trap the search in local optima, we adopt a random restart technique (Yagiura and Ibaraki 2001): sample M target tasks as initial centroids, locally refine each by the clustering loss above, and choose the one with the lowest loss as the training task for that round. We repeat this procedure for K rounds, training a policy on each selected task and evaluating it on all targets. Full algorithms, including our techniques to reduce the time complexity, are provided in Appendix H.1. We also provide a comparison between M-MBTL and GP-MBTL in Appendix J.

Algorithm 1: M/GP-MBTL

```

Input: Task set  $Y = \{y_n\}_{n \in [N]}$ 
for  $k \in [K]$  do
     $s = \text{Detect}(\{J(\pi_\kappa, y_n)\}_{n \in [N], \kappa \in [k-1]})$ 
    if  $s = \text{MOUNTAIN}$  then
         $x_k \leftarrow \text{Run M-MBTL}$ 
    else
         $x_k \leftarrow \text{Run GP-MBTL}$ 
    end if
    Train on  $x_k$ , receive  $\{J(\pi_k, y_n)\}_{n \in [N]}$ 
end for

```

4.4 M/GP-MBTL

Based on the two algorithms and the detection approach above, we introduce a concrete instantiation of SD-MBTL, named M/GP-MBTL (Algorithm 1). This algorithm uses the function $\text{Detect}(\cdot)$ mentioned in Section 4.2 to detect the problem structure. Then it dynamically chooses between M-MBTL for MOUNTAIN structures and GP-MBTL for more general settings, enabling the algorithm to tailor its task selection strategy to the underlying CMDP structure.

5 Experiments

In this section, we present an extensive evaluation of our approaches, organized around two guiding questions: **Q1**: Under what conditions does M-MBTL perform well, and under what conditions does GP-MBTL perform well? **Q2**: Can M/GP-MBTL always achieve the best of both worlds, or approach optimal performance? We investigate these questions on CMDP experiments, including synthetic data, continuous control, eco-friendly traffic control, and crop management. Appendix O.3 reports ablation studies to assess how different combinations of algorithms in SD-MBTL affect performance, and Appendix H.3 compares the runtime. Appendix O.2 shows the algorithm selection at each round and the number of training policies required to achieve ϵ -suboptimal.

To evaluate the performance of our algorithm in higher-dimensional settings, we conducted experiments on 5-dimensional and 7-dimensional synthetic datasets, which demonstrate the generalizability of M/GP-MBTL for multi-dimensional CMDP problems. Detailed results are provided in Appendix O.5. Moreover, to show that the decision-round parameter K in our results is not cherry-picked, we provide curves of the aggregated metrics as K varies in Appendix O.1 and O.2. After only a small number of decision rounds, M/GP-MBTL consistently maintains the best overall performance, demonstrating its robustness.

5.1 Setup

Although our aim is to tackle high-dimensional CMDPs, the number of tasks—and hence the training time—grows exponentially with dimensionality. Therefore, we confine our experiments to three-dimensional settings.

Baselines. We consider two types of baselines: canonical and multi-policy. The canonical baselines include: (1) **Independent training**, which trains separate policies on each MDP task; and (2) **Multi-task training**, where a universal context-conditioned policy is trained for all tasks. The multi-policy baselines include: (3) **Random selection**, which selects training tasks uniformly at random; (4) **GP-MBTL** (Cho et al. 2024); (5) **M-MBTL**; and (6) **Myopic Oracle**, an optimal solution for GSTS problem which has access to the generalization performance of each source-target pair (x, y) in all experiment trials and selects the training task myopically in each step. More details, including the formal definition and relationship to prior work, are provided in Appendix L.

Train and zero-shot transfer. We discretize the continuous task set X into N tasks. For the ease of our problem, we set these discretized tasks the same as Y . We use Proximal Policy Optimization (PPO) (Schulman et al. 2017) for training. We zero-shot transfer the policies obtained after training each task to all other tasks. The generalization performance constructs a transfer matrix whose rows represent source tasks and columns represent target tasks. We set the number of decision rounds $K = N$, and train three times with different random seeds. More details on deep RL implementation and hyperparameters are provided in Appendix N.

Bootstrapping. However, three matrices are not enough for evaluating our different source task selections. To address this, we employ *bootstrapping* (Tibshirani and Efron 1993) to synthesize an expanded dataset. Since each task is independently trained three times, the rows of the transfer matrix are independent. Therefore, we generate 100 bootstrapped transfer matrices with different random seeds by resampling rows of the transfer matrices with replacement from the original set of trained policies. Through bootstrapping, each row of the transfer matrix is still sampled from its true distribution, but the number of transfer matrices is significantly increased. It allows us to more reliably approximate the real distribution of the transfer matrix and thereby mitigate the effects of limited training runs.

Performance measure. We apply min-max normalization to the performance across all tasks after the algorithm is run. We use the mean as the performance metric, and use bootstrap

resampling to compute the 95% confidence intervals (CI) of the performance. Because the upper and lower bounds of the CI are roughly symmetric, we only display $\pm \frac{(\text{upper}-\text{lower})}{2}$ as the CI half-width. We also evaluated the IQM and the median of the performance, which are presented in Appendix O.2. Both of them are close to the mean. Additionally, to compare methods across different benchmarks and cases, we use an **aggregated performance** metric adapted from the human-normalized score (Badia et al. 2020; Mnih et al. 2015): each algorithm’s score on a benchmark is linearly rescaled so that the Random baseline maps to 0 and the Myopic Oracle to 1, and we then average these normalized scores over all benchmarks. This single 0–1 value shows both how much an algorithm surpasses Random and how close it comes to the oracle; full definitions and formulas appear in Appendix M.

5.2 Synthetic Data

Data description. We first evaluate the performance of M/GP-MBTL under synthesized dataset, including the cases where Assumptions 4.1 and 4.2 are satisfied or not, as well as cases with varying noise levels. We discretize the three dimensional continuous task set X into $N = 8 \times 8 \times 8$ tasks, each characterized by three context dimensions, where each dimension is an integer ranging from 1 to 8. We generate $J(\pi_x, y) = f(x) + g(y) + h(x, y) + C + \epsilon_{x,y}$, where $C = 500$ is a constant that does not affect any algorithmic decisions, $\epsilon_{x,y} \sim \mathcal{N}(0, \sigma^2)$ is a Gaussian noise sampled independently for all x and y , and $\sigma = 5$. We include eight conditions, which is the combination of three variations: 1) constant and non-constant $f(x)$; 2) constant and non-constant $g(y)$; 3) distance metric holds or does not hold. We use a linear function $f(x) = [4, 4, 4] \cdot x$ and $g(y) = [3, 3, 3] \cdot y$ for the non-constant case, and $f(x) = 0$, $g(y) = 0$ for constant case. When the distance metric holds, $h(x, y) = -[3, 3, 3] \cdot |x - y|$, where $|\cdot|$ means the absolute value for each element in a vector. Otherwise, $h(x, y) = -([3, 3, 3] \cdot [x - y]_+ + [1, 1, -3] \cdot [x - y]_-)$. We also tested our approaches on the synthetic data with different noise levels in Appendix O.1.

Results. Table 1 presents the performance comparison on synthetic data. Rows shaded in light gray indicate the synthetic settings that satisfy our proposed MOUNTAIN structure assumption. **Answer to Q1:** When MOUNTAIN structure holds, M-MBTL achieves the best performance among multi-policy baselines and closely approaches the performance of the myopic oracle. This indicates that M-MBTL effectively exploits this structure to get near-optimal performance with reduced training cost. Conversely, when MOUNTAIN structure is violated, GP-MBTL achieves the highest performance, demonstrating a general ability to handle CMDP problems. **Answer to Q2:** Overall, M/GP-MBTL attains the best aggregated performance, demonstrating that it can successfully detect whether a CMDP satisfies MOUNTAIN structure and choose the appropriate algorithm accordingly.

5.3 CMDP Benchmarks

Benchmarks. We consider four CMDP benchmarks: CartPole, BipedalWalker, IntersectionZoo, and CyclesGym. In CartPole, the objective is to keep a pole balanced upright

on a moving cart. We vary three key context variables—length of the pole, mass of the pole, and mass of the cart—in ranges spanning from 0.2 to 2 times their standard values ($N = 9 \times 10 \times 10$). BipedalWalker is a 4-joint walker robot environment. Context variables are friction, gravity, and scale, ranging from 0.2 to 1.6 times their default values ($N = 8 \times 8 \times 8$). We use CRL environments (Benjamins et al. 2023) for these CartPole and BipedalWalker. IntersectionZoo (Jayawardana et al. 2025) is a multi-agent CRL benchmark for eco-driving in urban road networks. We run experiments on a synthetic intersection network configuration with three context variables—traffic inflow, autonomous vehicle (AV) penetration rate, and traffic signal green-phase duration—from 0.2 to 1.2 times their default values ($N = 6 \times 6 \times 6$), providing a broad range of complex traffic scenarios for evaluation. CyclesGym (Turchetta et al. 2022) is an agricultural management simulation environment in which an RL agent is tasked with managing various crop-related parameters. Context variables are temperature, sunlight, and precipitation. These variables are discretized into a $6 \times 6 \times 6$ grid, yielding different agricultural scenarios. More details on CMDP benchmarks are provided in Appendix N.2.

Results. Table 2 summarizes the results across four benchmarks. **Answer to Q1:** On the whole, the gap between the Myopic Oracle and canonical baselines (independent and multi-task training) indicate the potential of MBTL-based strategic task selection. Multi-task training performs the best on CartPole, which may be because the problem is relatively easy, such that a single straightforward context-conditioned policy can achieve strong performance across the CMDP. However, it performs worse in other benchmarks, potentially due to increased task complexity, where it may suffer from model capacity limitations. By contrast, M-MBTL and GP-MBTL show better aggregated metric performance than independent training and multi-task training. In tasks that satisfy MOUNTAIN structure (BipedalWalker, CyclesGym), M-MBTL achieves the highest performance. When the structure is violated (IntersectionZoo), GP-MBTL becomes superior, showing the value of a GP model for source-task performance. In addition, CartPole satisfies the assumptions of both M-MBTL and GP-MBTL, so both algorithms perform well. **Answer to Q2:** Across all four benchmarks, M/GP-MBTL consistently matches the stronger of M-MBTL and GP-MBTL. It achieves the best aggregated performance and shows an improvement of 0.1249 over GP-MBTL, indicating that it moves 12.49% closer to the Myopic Oracle within the MBTL framework. This highlights the method’s effectiveness in addressing various CMDP problems.

6 Related Works

Contextual Reinforcement Learning and Multi-Policy Approaches. CRL provides a framework for managing variations of MDP in environment dynamics, rewards, and initial states through a context variable, effectively yielding a family of related tasks parameterized by these contexts (Hallak, Di Castro, and Mannor 2015; Modi et al. 2018; Benjamins et al. 2023). When the context is observed, a popular approach is to train a single policy that explicitly conditions on this contextual information (Teh et al. 2017; Sodhani, Zhang,

$f(x)$	$g(y)$	$h(x, y)$	Random	GP-MBTL	M-MBTL (Ours)	M/GP-MBTL (Ours)	Myopic Oracle
Constant	Linear	Non-distance	0.6956 ± 0.0009	0.7212 ± 0.0006	0.6976 ± 0.0002	0.7168 ± 0.0010	0.7260 ± 0.0001
Constant	Linear	L_1 norm	0.7011 ± 0.0002	0.6961 ± 0.0011	0.7038 ± 0.0002	0.7038 ± 0.0002	0.7048 ± 0.0002
Constant	None	Non-distance	0.7906 ± 0.0014	0.8369 ± 0.0003	0.7936 ± 0.0003	0.8334 ± 0.0004	0.8375 ± 0.0002
Constant	None	L_1 norm	0.7722 ± 0.0004	0.7747 ± 0.0005	0.7762 ± 0.0003	0.7762 ± 0.0003	0.7778 ± 0.0003
Linear	Linear	Non-distance	0.5773 ± 0.0015	0.6088 ± 0.0001	0.5782 ± 0.0001	0.6086 ± 0.0001	0.6090 ± 0.0001
Linear	Linear	L_1 norm	0.5880 ± 0.0020	0.6218 ± 0.0001	0.5900 ± 0.0002	0.6216 ± 0.0002	0.6221 ± 0.0001
Linear	None	Non-distance	0.6672 ± 0.0020	0.7083 ± 0.0002	0.6683 ± 0.0002	0.7073 ± 0.0006	0.7088 ± 0.0002
Linear	None	L_1 norm	0.7401 ± 0.0021	0.7744 ± 0.0012	0.7422 ± 0.0002	0.7751 ± 0.0002	0.7756 ± 0.0001
Aggregated Performance			-0.0000 ± 0.0107	0.2127 ± 0.0511	0.0147 ± 0.0089	0.3099 ± 0.0290	1.0000 ± 0.0088

Table 1: Performance comparison on Synthetic Data ($\epsilon = \mathcal{N}(0, 5^2)$) with $K = 50$. Values are reported as the mean performance \pm half the width of the 95% confidence interval. Rows shaded in gray indicate the settings that satisfy our proposed MOUNTAIN structure. Bold values represent the highest value(s) within the statistically significant range for each task, excluding the oracle.

Benchmark (CMDP)	Independent	Multi-task	Random	GP-MBTL	M-MBTL (Ours)	M/GP-MBTL (Ours)	Myopic Oracle
CartPole	0.9346	0.9967	0.9861	0.9919	0.9896	0.9898	0.9998
$(K = 12)$	± 0.0003	± 0.0024	± 0.0017	± 0.0013	± 0.0016	± 0.0016	± 0.0000
BipedalWalker	0.7794	0.5680	0.8051	0.8073	0.8315	0.8261	0.8629
$(K = 12)$	± 0.0011	± 0.0919	± 0.0045	± 0.0044	± 0.0029	± 0.0030	± 0.0011
IntersectionZoo	0.2045	0.3788	0.5288	0.5840	0.4878	0.5682	0.6305
$(K = 50)$	± 0.0008	± 0.1059	± 0.0108	± 0.0092	± 0.0064	± 0.0069	± 0.0082
CyclesGym	0.2133	0.2081	0.2198	0.2193	0.2205	0.2201	0.2214
$(K = 50)$	± 0.0002	± 0.0002	± 0.0001	± 0.0001	± 0.0001	± 0.0001	± 0.0001
Aggregated Performance	-2.9063	-3.1120	0.0000	0.1681	0.1822	0.2930	1.0000
	± 0.1470	± 1.8408	± 0.0467	± 0.0539	± 0.0503	± 0.0403	± 0.0236

Table 2: Performance comparison of different methods on CMDP benchmarks. Values are reported as the mean performance \pm half the width of the 95% confidence interval. Bold values represent the highest value(s) within the statistically significant range for each task, excluding the oracle.

and Pineau 2021) or by encoding it with a latent representation (Yu et al. 2020; Sun et al. 2022). Although performance can be strong when the tasks are homogeneous, negative transfer and capacity limits arise when context variation is large. An alternative is to train a small set of expert policies. This idea has been explored through policy committees (Ge et al. 2025) and represented-MDPs (Ivanov and Ben-Porat 2024), where the primary goal is to cluster the task space upfront and train one expert policy per cluster. Recent work shows that training only a few carefully chosen source tasks can outperform both independent training and multi-task training (Cho et al. 2023, 2024). We generalize these ideas in multi-dimensional contexts and a *meta* layer that first detects what generalization structure is present before choosing which task-selection to deploy.

Structure Detection. Structure detection appears widely in machine learning, for example in detecting convexity for optimization problems (Ahmadi et al. 2013) and discovering GP kernels for nonparametric regression (Duvenaud et al. 2013). Typical frameworks include finding good approximations or decomposing the unknown functions. However, structure detection is fairly nascent in the context of CRL. In CRL, structure detection appears as (i) *context change detection*, where hierarchical RL agents infer when environment dynamics have shifted and switch options accordingly

(Yücesoy and Tümer 2015); (ii) *model selection*, where online statistical tests reject over-complex dynamics models to curb over-fitting (Lee et al. 2021); and (iii) *policy-reuse selection*, where an agent leverages a pre-existing library of policies. These methods decide whether a source policy can be safely transferred to a new target task (Fernández and Veloso 2006) or combine multiple source policies to solve a target task, for example, through a mixture-of-experts model (Gimelfarb, Sanner, and Lee 2021). Our work also detects structure online, but we leverage it to choose a source-task, rather than to re-weight or gate a fixed library of policies; in principle, both ideas can be combined.

Appendix A surveys additional literature on clustering methods and solutions for CRL.

7 Conclusion

We propose a structure detection framework for CRL that infers the underlying structure of CMDPs and adaptively selects the task selection strategy. Our M/GP-MBTL algorithm switches between a clustering strategy for MOUNTAIN cases and a GP-based strategy otherwise. Experiments on synthetic and real benchmarks show consistent improvements over prior methods, highlighting the promise of structure detection for scalable and robust transfer learning in complex CRL environments. Nevertheless, our study has several

limitations. First, the current detector focuses on a single structure; Second, structure inference relies on transfer evaluations of training tasks, which can be costly when the context space is very large or when policies are expensive to evaluate; Third, all experiments were conducted in three-dimensional context spaces; additional work is needed to confirm scalability to higher-dimensional settings. Future work will explore richer CMDP structures and develop specialized algorithms to reduce the number of required source-task trainings while maintaining (or improving) generalization performance.

Acknowledgements

This work was supported by the National Science Foundation (NSF) CAREER award (#2239566) and the Kwanjeong Educational Foundation Ph.D. scholarship program. The authors would like to thank the anonymous reviewers for their valuable feedback.

References

Agarwal, R.; Schwarzer, M.; Castro, P. S.; Courville, A.; and Bellemare, M. G. 2021a. Deep reinforcement learning at the edge of the statistical precipice. In *Proceedings of the 35th International Conference on Neural Information Processing Systems*, NIPS '21. Red Hook, NY, USA: Curran Associates Inc. ISBN 9781713845393.

Agarwal, R.; Schwarzer, M.; Castro, P. S.; Courville, A. C.; and Bellemare, M. 2021b. Deep reinforcement learning at the edge of the statistical precipice. *Advances in neural information processing systems*, 34: 29304–29320.

Ahmadi, A. A.; Olshevsky, A.; Parrilo, P. A.; and Tsitsiklis, J. N. 2013. NP-hardness of deciding convexity of quartic polynomials and related problems. *Mathematical programming*, 137: 453–476.

Arthur, D.; and Vassilvitskii, S. 2007. k-means++: the advantages of careful seeding. In *Proceedings of the Eighteenth Annual ACM-SIAM Symposium on Discrete Algorithms*, SODA '07, 1027–1035. USA: Society for Industrial and Applied Mathematics. ISBN 9780898716245.

Badia, A. P.; Piot, B.; Kapturowski, S.; Sprechmann, P.; Vitvitskyi, A.; Guo, D.; and Blundell, C. 2020. Agent57: outperforming the Atari human benchmark. In *Proceedings of the 37th International Conference on Machine Learning*, ICML'20. JMLR.org.

Bellemare, M. G.; Candido, S.; Castro, P. S.; Gong, J.; Machado, M. C.; Moitra, S.; Ponda, S. S.; and Wang, Z. 2020. Autonomous navigation of stratospheric balloons using reinforcement learning. *Nature*, 588(7836): 77–82.

Benjamins, C.; Eimer, T.; Schubert, F.; Mohan, A.; Döhler, S.; Biedenkapp, A.; Rosenhahn, B.; Hutter, F.; and Lindauer, M. 2023. Contextualize Me – The Case for Context in Reinforcement Learning. *Transactions on Machine Learning Research*.

Cho, J.-H.; Jayawardana, V.; Li, S.; and Wu, C. 2024. Model-Based Transfer Learning for Contextual Reinforcement Learning. In *Advances in Neural Information Processing Systems*, volume 37, 88279–88319. Curran Associates, Inc.

Cho, J.-H.; Li, S.; Kim, J.; and Wu, C. 2023. Temporal Transfer Learning for Traffic Optimization with Coarse-grained Advisory Autonomy. *arXiv:2312.09436*.

Defays, D. 1977. An efficient algorithm for a complete link method. *The computer journal*, 20(4): 364–366.

Degrave, J.; Felici, F.; Buchli, J.; Neunert, M.; Tracey, B.; Carpanese, F.; Ewalds, T.; Hafner, R.; Abdolmaleki, A.; de Las Casas, D.; et al. 2022. Magnetic control of tokamak plasmas through deep reinforcement learning. *Nature*, 602(7897): 414–419.

Dempster, A. P.; Laird, N. M.; and Rubin, D. B. 1977. Maximum likelihood from incomplete data via the EM algorithm. *Journal of the Royal Statistical Society: Series B (Methodological)*, 39(1): 1–22.

Dennis, M.; Jaques, N.; Vinitsky, E.; Bayen, A.; Russell, S.; Critch, A.; and Levine, S. 2020. Emergent complexity and zero-shot transfer via unsupervised environment design. *Advances in neural information processing systems*, 33: 13049–13061.

Duvenaud, D.; Lloyd, J.; Grosse, R.; Tenenbaum, J.; and Zoubin, G. 2013. Structure discovery in nonparametric regression through compositional kernel search. In *International Conference on Machine Learning*, 1166–1174. PMLR.

Eimer, T.; Biedenkapp, A.; Hutter, F.; and Lindauer, M. 2021. Self-paced context evaluation for contextual reinforcement learning. In *International Conference on Machine Learning*, 2948–2958. PMLR.

Fernández, F.; and Veloso, M. 2006. Probabilistic policy reuse in a reinforcement learning agent. In *Proceedings of the fifth international joint conference on Autonomous agents and multiagent systems*, 720–727.

Finn, C.; Abbeel, P.; and Levine, S. 2017. Model-agnostic meta-learning for fast adaptation of deep networks. In *International conference on machine learning*, 1126–1135. PMLR.

Gardner, J. R.; Pleiss, G.; Bindel, D.; Weinberger, K. Q.; and Wilson, A. G. 2018. GPyTorch: blackbox matrix-matrix Gaussian process inference with GPU acceleration. In *Proceedings of the 32nd International Conference on Neural Information Processing Systems*, NIPS'18, 7587–7597. Red Hook, NY, USA: Curran Associates Inc.

Ge, L.; Lanier, M.; Sarkar, A.; Guresti, B.; Zhang, C.; and Vorobeychik, Y. 2025. Learning Policy Committees for Effective Personalization in MDPs with Diverse Tasks. In *Forty-second International Conference on Machine Learning*.

Gimelfarb, M.; Sanner, S.; and Lee, C.-G. 2021. Contextual policy transfer in reinforcement learning domains via deep mixtures-of-experts. In de Campos, C.; and Maathuis, M. H., eds., *Proceedings of the Thirty-Seventh Conference on Uncertainty in Artificial Intelligence*, volume 161 of *Proceedings of Machine Learning Research*, 1787–1797. PMLR.

Hallak, A.; Di Castro, D.; and Mannor, S. 2015. Contextual markov decision processes. *arXiv preprint arXiv:1502.02259*.

Hendawy, A.; Peters, J.; and D'Eramo, C. 2023. Multi-task reinforcement learning with mixture of orthogonal experts. *arXiv preprint arXiv:2311.11385*.

Hoeffding, W. 1948. A class of statistics with asymptotic normal distribution. *Annals of Mathematical Statistics*, 19: 293–325.

Ivanov, D.; and Ben-Porat, O. 2024. Personalized reinforcement learning with a budget of policies. In *Proceedings of the AAAI Conference on Artificial Intelligence*, volume 38, 12735–12743.

Jain, A. K.; and Dubes, R. C. 1988. *Algorithms for clustering data*. Prentice-Hall, Inc.

Jayawardana, V.; Freydt, B.; Qu, A.; Hickert, C.; Yan, Z.; and Wu, C. 2025. IntersectionZoo: Eco-driving for Benchmarking Multi-Agent Contextual Reinforcement Learning. In *The Thirteenth International Conference on Learning Representations*.

Kang, Z.; Grauman, K.; and Sha, F. 2011. Learning with whom to share in multi-task feature learning. In *Proceedings of the 28th International Conference on Machine Learning (ICML-11)*, 521–528.

Klink, P.; D'Eramo, C.; Peters, J. R.; and Pajarinen, J. 2020. Self-paced deep reinforcement learning. *Advances in Neural Information Processing Systems*, 33: 9216–9227.

Lee, J.; Pacchiano, A.; Muthukumar, V.; Kong, W.; and Brunskill, E. 2021. Online model selection for reinforcement learning with function approximation. In *International Conference on Artificial Intelligence and Statistics*, 3340–3348. PMLR.

Lopez, P. A.; Behrisch, M.; Bieker-Walz, L.; Erdmann, J.; Flötteröd, Y.-P.; Hilbrich, R.; Lücken, L.; Rummel, J.; Wagner, P.; and Wießner, E. 2018. Microscopic Traffic Simulation using SUMO. In *The 21st IEEE International Conference on Intelligent Transportation Systems*. IEEE.

MacQueen, J.; et al. 1967. Some methods for classification and analysis of multivariate observations. In *Proceedings of the fifth Berkeley symposium on mathematical statistics and probability*, volume 1, 281–297. Oakland, CA, USA.

Mnih, V.; Kavukcuoglu, K.; Silver, D.; Rusu, A. A.; Veness, J.; Bellemare, M. G.; Graves, A.; Riedmiller, M. A.; Fidjeland, A. K.; Ostrovski, G.; Petersen, S.; Beattie, C.; Sadik, A.; Antonoglou, I.; King, H.; Kumaran, D.; Wierstra, D.; Legg, S.; and Hassabis, D. 2015. Human-level control through deep reinforcement learning. *Nature*, 518: 529–533.

Modi, A.; Jiang, N.; Singh, S.; and Tewari, A. 2018. Markov decision processes with continuous side information. In *Algorithmic Learning Theory*, 597–618. PMLR.

Narvekar, S.; Peng, B.; Leonetti, M.; Sinapov, J.; Taylor, M. E.; and Stone, P. 2020. Curriculum learning for reinforcement learning domains: A framework and survey. *Journal of Machine Learning Research*, 21(181): 1–50.

Nielsen, F. 2016. *Hierarchical Clustering*, 195–211. ISBN 978-3-319-21902-8.

Raffin, A.; Hill, A.; Gleave, A.; Kanervisto, A.; Ernestus, M.; and Dormann, N. 2021. Stable-Baselines3: Reliable Reinforcement Learning Implementations. *Journal of Machine Learning Research*, 22(268): 1–8.

Schulman, J.; Wolski, F.; Dhariwal, P.; Radford, A.; and Klimov, O. 2017. Proximal policy optimization algorithms. *arXiv preprint arXiv:1707.06347*.

Sobol', I. M. 1990. On sensitivity estimation for nonlinear mathematical models. *Matematicheskoe modelirovaniye*, 2(1): 112–118.

Sodhani, S.; Zhang, A.; and Pineau, J. 2021. Multi-task reinforcement learning with context-based representations. In *International Conference on Machine Learning*, 9767–9779. PMLR.

Standley, T.; Zamir, A.; Chen, D.; Guibas, L.; Malik, J.; and Savarese, S. 2020. Which Tasks Should Be Learned Together in Multi-task Learning? In III, H. D.; and Singh, A., eds., *Proceedings of the 37th International Conference on Machine Learning*, volume 119 of *Proceedings of Machine Learning Research*, 9120–9132. PMLR.

Sun, L.; Zhang, H.; Xu, W.; and Tomizuka, M. 2022. Paco: Parameter-compositional multi-task reinforcement learning. *Advances in Neural Information Processing Systems*, 35: 21495–21507.

Szekely, G. J.; Rizzo, M. L.; et al. 2005. Hierarchical clustering via joint between-within distances: Extending Ward's minimum variance method. *Journal of classification*, 22(2): 151–184.

Teh, Y.; Bapst, V.; Czarnecki, W. M.; Quan, J.; Kirkpatrick, J.; Hadsell, R.; Heess, N.; and Pascanu, R. 2017. Distral: Robust multitask reinforcement learning. *Advances in neural information processing systems*, 30.

Tibshirani, R. J.; and Efron, B. 1993. An introduction to the bootstrap. *Monographs on statistics and applied probability*, 57(1): 1–436.

Turchetta, M.; Corinzia, L.; Sussex, S.; Burton, A.; Herrera, J.; Athanasiadis, I.; Buhmann, J. M.; and Krause, A. 2022. Learning long-term crop management strategies with cyclesgym. *Advances in neural information processing systems*, 35: 11396–11409.

Yagiura, M.; and Ibaraki, T. 2001. On Metaheuristic Algorithms for Combinatorial Optimization Problems. *Systems and Computers in Japan*, 32.

Yu, T.; Quillen, D.; He, Z.; Julian, R.; Hausman, K.; Finn, C.; and Levine, S. 2020. Meta-world: A benchmark and evaluation for multi-task and meta reinforcement learning. In *Conference on robot learning*, 1094–1100. PMLR.

Yücesoy, Y. E. Y.; and Tümer, M. B. 2015. Hierarchical Reinforcement Learning with Context Detection (HRL-CD). *International Journal of Machine Learning and Computing*, 5(5): 353–358.

Čech, E.; and Katětov, M. 1969. *Point Sets*. Academia, Publishing House of the Czechoslovak Academy of Sciences.

Appendix

A Additional Related Works

Clustering. Clustering is a fundamental technique for grouping unlabeled data by similarity (MacQueen et al. 1967; Dempster, Laird, and Rubin 1977; Arthur and Vassilvitskii 2007). Hierarchical clustering extends this principle by splitting or merging clusters dynamically, allowing a flexible number of centroids (Defays 1977; Szekely, Rizzo et al. 2005; Nielsen 2016). M-MBTL further adapts clustering to an iterative setting: it incrementally adds new centroids while preserving previously learned ones, providing an efficient way to guide the search for training tasks in the GSTS problem.

Multi-task Training. Multi-task RL seeks to learn a single policy (or a set of shared parameters) to solve *multiple related tasks* (Teh et al. 2017; Sodhani, Zhang, and Pineau 2021). While multi-task methods such as PaCo (Sun et al. 2022) and MOORE (Hendawy, Peters, and D’Eramo 2023) have demonstrated success in discrete and continuous domains, they often assume a fixed task set and can suffer from negative transfer when certain tasks are too dissimilar (Kang, Grauman, and Sha 2011; Standley et al. 2020).

Curriculum and Self-Paced Learning. Task-selection for multi-policy training is closely related to curriculum learning for RL, where an agent is exposed to an automatically ordered sequence of source tasks (Narvekar et al. 2020). Another related approach called self-paced learning selects only a few representative task instances to train on (Klink et al. 2020; Eimer et al. 2021). Whereas curriculum methods aim to ease online learning of a *single* policy, our goal is to minimize the number of expensive training runs by deciding *which* contexts to fully train on for zero-shot transfer. In addition, curriculum learning or self-paced learning typically aims to accelerate the online training of a single universal policy, while our framework focuses on minimizing the total, often computationally prohibitive, cost of training by selecting an optimal subset of source tasks for training multiple expert policies that provide broad zero-shot coverage.

Unsupervised Environment Design (UED). UED methods automatically generate training tasks whose difficulty adapts to the current agent, producing curricula without hand-crafted ordering rules. ACCEL (Dennis et al. 2020) formulates environment creation as an RL problem whose reward is tasks on the brink of the agent’s competence. These works complement ours: they invent new source tasks, whereas we select from a fixed CMDP. Our structure detection could, in principle, guide a UED generator—e.g. to bias sampling toward contexts that satisfy a detected MOUNTAIN structure.

Meta-learning. Meta-RL algorithms such as MAML (Finn, Abbeel, and Levine 2017) learn policies that adapt rapidly to a *single* new task via a few gradient steps or a short context window. Our method differs in motivation: we want *zero-shot* coverage of *all* tasks in a CMDP while minimizing the number of full training runs. Nevertheless, meta-learning could boost each individual source-task training phase, and conversely our structure detector could decide *when* to switch from meta-learning to plain fine-tuning as context variance grows.

B Notation Table

Table 3 describes the notation used in this paper.

Table 3: Notation Table

Symbol	Description
x	Source task ($x \in \mathcal{X}$)
y	Target task ($y \in \mathcal{Y}$)
π_x	Trained policy from source task
$J(\pi_x, y)$	Generalization Performance of π_x on y
$x_{1:K}$	Selected source tasks x_1, x_2, \dots, x_K
$f(x)$	Policy quality of source task x
$g(y)$	Difficulty of target task y
$h(x, y)$	Task dissimilarity between x and y
$\text{dist}(x, y)$	A distance metric
$\bar{J}(\pi_x, y)$	Relative generalization performance of π_x on y

C Details of the Generalization-Performance Structure Decomposition

The Sobol–Hoeffding (functional-ANOVA) decomposition provides a *unique* and *orthogonal* expansion of any square-integrable function of *independent* inputs into a grand mean, additive main-effect terms, and a residual interaction term. We restate the result for the two-variable case, which underpins our generalization-performance model.

Theorem C.1 (Sobol–Hoeffding decomposition for two variables (Hoeffding 1948; Sobol’ 1990)). *Let (X, Y) be independent random variables with supports \mathcal{X} and \mathcal{Y} , and let $F \in L^2(\mathcal{X} \times \mathcal{Y})$. Define the global mean*

$$\mu = \mathbb{E}_{X,Y}[F(X, Y)].$$

Then there exist unique functions $F_X \in L^2(\mathcal{X})$, $F_Y \in L^2(\mathcal{Y})$, $F_{XY} \in L^2(\mathcal{X} \times \mathcal{Y})$ such that

$$F(x, y) = \mu + F_X(x) + F_Y(y) + F_{XY}(x, y),$$

with the orthogonality and zero-mean conditions

$$\mathbb{E}_X[F_X(X)] = \mathbb{E}_Y[F_Y(Y)] = \mathbb{E}_{X,Y}[F_{XY}(X, Y)] = 0.$$

Explicitly,

$$\begin{aligned} F_X(x) &= \mathbb{E}_Y[F(x, Y)] - \mu, \\ F_Y(y) &= \mathbb{E}_X[F(X, y)] - \mu, \end{aligned} \tag{7}$$

$$F_{XY}(x, y) = F(x, y) - F_X(x) - F_Y(y) - \mu.$$

Connection to Definition 3.1. Let $J(\pi_x, y)$ denote the generalization-performance function and identify $F(x, y) = J(\pi_x, y)$. Set $g(y) := F_Y(y)$ and introduce

$$\begin{aligned} f(x) &:= F_X(x) - F_{XY}(x, x), \\ h(x, y) &:= J(\pi_x, y) - f(x) - g(y) - \mu. \end{aligned} \tag{8}$$

This construction yields exactly the decomposition stated in Definition 3.1. It also leads to a difference between the Sobol-Hoeffding decomposition and our definition. Because the diagonal term $F_{XY}(x, x)$ is subtracted from $F_X(x)$, the interaction term is normalized so that $h(x, y) = 0$ if $x = y$. However, $\mathbb{E}_x[f(x)] = 0$ is not satisfied.

D Proof of Equivalence in Definition 4.3

Proof. The equivalent relationship is because, since $f(x) = C_1$ and $h(x, y) = -\text{dist}(x, y)$, we can get $J(\pi_y, y) = g(y) + C_1 + C$. Therefore, $J(\pi_x, y) = C_1 + C + (J(\pi_y, y) - C_1 - C) - \text{dist}(x, y) = J(\pi_y, y) - \text{dist}(x, y)$. \square

E Proof of Lemma 4.4

Proof. Since $h(x, y) = 0$ if $x = y$, we can get $\bar{J}(\pi_x, x) = f(x)$. Therefore, $\text{std}_{x \in x_{1:k}}(\bar{J}(\pi_x, x)) = \text{std}_{x \in x_{1:k}}(f(x))$, and $\text{std}_{y \in Y}(\bar{J}(\pi_x, y)) = \text{std}_{y \in Y}(h(x, y))$. Thus, if $\text{std}_{x \in x_{1:k}}(\bar{J}(\pi_x, x)) < \mathbb{E}_{x \in x_{1:k}}[\text{std}_{y \in Y}(\bar{J}(\pi_x, y))]$, we have $\text{std}_{x \in x_{1:k}}(f(x)) < \mathbb{E}_{x \in x_{1:k}}[\text{std}_{y \in Y}(h(x, y))]$. \square

F Proof of Lemma 4.5

Lemma 4.5 shows that if Mountain structure holds, we have $J(\pi_x, y) = J(\pi_y, y) - \text{dist}(x, y)$. The GSTS problem can be reduced to a sequential version of clustering. Here is a proof.

Proof.

$$\begin{aligned} & \max_{x_k} \mathbb{E}_{y_n \in \mathcal{U}(Y)} [\max_{\kappa \in [k]} J(\pi_{x_\kappa}, y_n)] \\ &= \max_{x_k} \mathbb{E}_{y_n \in \mathcal{U}(Y)} [\max_{\kappa \in [k]} J(\pi_{y_n}, y_n) - \text{dist}(x_\kappa, y_n)] \quad (9) \\ & \Leftrightarrow -\min_{x_k} \mathbb{E}_{y_n \in \mathcal{U}(Y)} [\min_{\kappa \in [k]} \text{dist}(x_\kappa, y_n)] \end{aligned}$$

\square

G Details in Slope Criterion

Below, we provide more details on calculating the slopes in Slope Criterion. First, we concatenate the context difference as $\text{diff}_{\kappa, n} = [[x_\kappa - y_n]_-, [x_\kappa - y_n]_+]$, $\forall \kappa, n$. Here we slightly abuse the notation that $[\cdot]_+$ and $[\cdot]_-$ represent $\max(\cdot, 0)$ and $\min(\cdot, 0)$ for each element in the vector, respectively. Using linear regression on the pairs $\{\bar{J}(\pi_{x_\kappa}, y_n)\}_{n \in [N], \kappa \in [k]}$ versus $\{\text{diff}_{\kappa, n}\}_{n \in [N], \kappa \in [k]}$, we obtain slopes from the left and right sides: $\theta_{\text{left}} \in \mathbb{R}^D$ and $\theta_{\text{right}} \in \mathbb{R}^D$.

H M-MBTL

H.1 Main Algorithm

We propose MOUNTAIN Model-Based Transfer Learning (M-MBTL, Algorithm 2) as a solution to GSTS, inspired by the K-Means clustering algorithm (MacQueen et al. 1967). However, K-Means and other traditional clustering methods (Dempster, Laird, and Rubin 1977; Jain and Dubes 1988; Arthur and Vassilvitskii 2007) do not support the sequential addition of centroids, where the added centroid corresponds to selecting a task for RL training. To address this limitation, we extend the traditional clustering algorithm into a sequential form. Given a task set $Y = \{y_n\}_{n \in [N]}$, M-MBTL proceeds through K decision rounds. In each round, M-MBTL aims to identify a new centroid as the training task x_k , while keeping the previous centroids $x_{1:k-1}$ fixed. However, this fixation of centroids—an important distinction between M-MBTL and traditional clustering—causes the new centroid to converge to a local optimum positioned

between the fixed centroids. To address this issue, we employ the random restart technique (Yagiura and Ibaraki 2001). This approach involves randomly sampling H task points $\{x_{k,m}^{\text{init}}\}_{m \in [M]}$ from the target task set Y , updating these candidates, and selecting the one with the best performance. During the call to $\text{Update}(x_{k,m}^{\text{init}}, x_{1:k-1})$, each initial candidate $x_{k,m}^{\text{init}}$ is added as a new centroid while the existing centroids $x_{1:k-1}$ remain fixed. We then refine this centroid by minimizing the clustering loss $\sum_{n=1}^N \min_{\kappa \leq k} \text{dist}(x_\kappa, y_n)$, yielding an updated candidate $x_{k,m}$ and its loss $l_{k,m}$. Full details appear in Algorithm 3. Figure 3 illustrates an overview of M-MBTL. M-MBTL selects the candidate with the lowest loss as the training task x_k . We introduce techniques to reduce the time complexity of M-MBTL, which are provided in Appendix H.2. We also have a comparison between M-MBTL and GP-MBTL, which is provided in Appendix J.

Algorithm 2: M-MBTL

Input: Task set $Y = \{y_n\}_{n \in [N]}$, number of samples M .
 $\{x_{k,m}^{\text{init}}\}_{m \in [M]} = \text{Sample}(Y, M)$
for $k \in [K]$ **do**
 for $m \in [M]$ **do**
 $x_{k,m}, l_{k,m} = \text{Update}(x_{k,m}^{\text{init}}, x_{1:k-1})$
 end for
 $x_k = x_{k, \arg \min_m l_{k,m}}$
 Train on x_k
end for

Algorithm 3: Update

Input: Initial point x^{init} , previous centroids $x_{1:k-1}$.
 $x_k = x^{\text{init}}$
while x_k not converged **do**
 for $n \in [N], \kappa \in [k]$ **do**
 $r_{n,\kappa} = \mathbb{I}(\kappa = \arg \max_{\kappa'} \text{dist}(x_\kappa, y_n))$
 end for
 $x_k = \arg \min_x \sum_{n \in [N]} r_{n,k} \text{dist}(x, y_n)$
end while
 $l_k = \sum_{n \in [N], \kappa \in [k]} r_{n,\kappa} \text{dist}(x_\kappa, y_n)$
Output: x_k, l_k

H.2 Reducing Time Complexity of M-MBTL

Since 1) M-MBTL uses a fixed set of M samples as initial candidates, and 2) only the centroid x_k needs to be updated in the update process, we can reduce the time complexity in two key ways. Specifically, we introduce Get Performance (Algorithm 4) to replace Update (Algorithm 3) in M-MBTL.

First, some redundant calculations can be avoided in this process by updating each initial candidate. For a candidate indexed by m ($m \in [M]$), its optimized version from the previous round is $x_{k-1,m}$. If the cluster of $x_{k-1,m}$ does not intersect with the previous training task x_{k-1} , this implies that the two centroids reduce the distances to different task points. In this case, we can leverage information from the

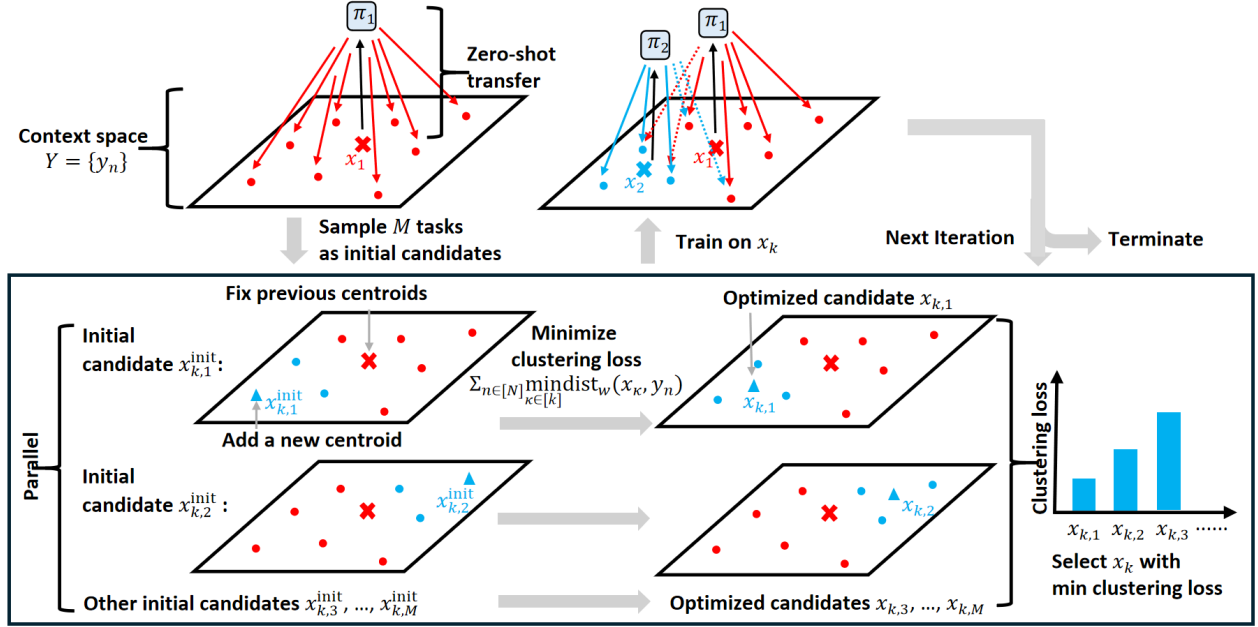


Figure 3: **Overview illustration for M-MBTL.** (a) A distance metric is used to estimate the generalization gaps between tasks and existing policies. (b) A random restart approach is employed to search for the next training task. M tasks are sampled as initial candidates, with each initial candidate serving as a new centroid candidate while previous centroids are fixed. The candidate is optimized based on the clustering loss, and the optimized candidate with the minimum loss is selected as the next training task. (c) Train on the selected task.

previous round to update $x_{k,m}$ and $l_{k,m}$. Specifically, we define $c(y_n, x_{1:k})$ as the cluster centroid of point y_n given all centroids $x_{1:k}$:

$$c(y_n, x_{1:k}) = \arg \min_{x_{\kappa} \in x_{1:k}} \text{dist}(x_{\kappa}, y_n) \quad (10)$$

Also, we define $\text{Intersect}(x_{k-1,i}, x_{1:k-1})$ as the indicator that the cluster of $x_{k-1,i}$ intersects with the cluster of x_{k-1} :

$$\begin{aligned} \text{Intersect}(x_{k-1,i}, x_{1:k-1}) \\ = \mathbb{I}(\exists n \in [N], c(y_n, x_{1:k-1}) = x_{k-1}, \\ c(y_n, x_{1:k-2} \cup x_{k-1,i}) = x_{k-1,i}) \end{aligned} \quad (11)$$

Define $\Delta l_k = l_k - l_{k-1}$ as the reduced loss at round k . If $\text{Intersect}(x_{k-1,m}, x_{1:k-1})$ is false, then $x_{k,m} = x_{k-1,m}$ and $l_{k,m} = l_{k-1,m} - \Delta l_{k-1}$, since the selected training task in this decision round and the previous round reduces the distances to different target tasks. Otherwise, we update $x_{k,m}$ and $l_{k,m}$ in the usual manner. The details are described in Algorithm 4.

Second, in the update process, since we only need to update x_k , we do not need to calculate the distances between all task points and centroids in each iteration. Instead, we only need to compute the distance for the (n, κ) pairs influenced by x_k . Define $S(r)$ as the set of (n, κ) pairs where we need to update the distances and labels:

$$\begin{aligned} S(r) = \{(n, \kappa) \mid (r_{n,k} = 1, \kappa \in [k]) \\ \text{or } (r_{n,k} = 0, \kappa \in \{k\} \cup \{\kappa' \mid r_{n,\kappa'} = 1\})\} \end{aligned} \quad (12)$$

Algorithm 4: Get Performance

Input: Initial point $x_{k,m}^{\text{init}}$, previous centroids $x_{1:k-1}$.
if not $\text{Intersect}(x_{k-1,m}, x_{1:k-1})$ **then**
 $x_{k,m} = x_{k-1,m}$
 $l_{k,m} = l_{k-1,m} - \Delta l_{k-1}$
else
 $x_{k,m}, l_{k,m} = \text{Fast Update}(x_{k,m}^{\text{init}}, x_{1:k-1})$
end if
Output: $x_{k,m}, l_{k,m}$

Here, $r_{n,k} = 1, \kappa \in [k]$ indicates that if the point x_n belongs to cluster k , we calculate its distance to all centroids. $r_{n,k} = 0, \kappa \in \{k\} \cup \{\kappa' \mid r_{n,\kappa'} = 1\}$ indicates that if x_n does not belong to cluster k , we only calculate its distance to its original centroid and the new centroid x_k . This approach reduces the time complexity. The details are described in Algorithm 5.

H.3 Time comparison

Figure 4 shows the CPU time comparison of M/GP-MBTL with M-MBTL and GP-MBTL. When k is small, M-MBTL has a slightly higher runtime than GP-MBTL. However, as k increases, M-MBTL exhibits significantly lower runtime compared to GP-MBTL. This is because GP-MBTL requires considerable time to estimate the Gaussian Process model when handling a large number of training tasks. The run-

Algorithm 5: Fast Update

Input: Initial point x^{init} , previous centroids $x_{1:k-1}$.
 $x_k = x^{\text{init}}$
 $d_{n,\kappa} = \text{dist}_{w_k}(x_\kappa, y_n), \forall n \in [N], \kappa \in [k]$
 $r_{n,\kappa} = \mathbb{I}(\kappa = \arg \max_{\kappa'} d_{n,\kappa}), \forall n \in [N], \kappa \in [k]$
while x_k not converged **do**
 $d_{n,\kappa} = \text{dist}_{w_k}(x_\kappa, y_n), \forall (n, \kappa) \in S(r)$
 $r_{n,\kappa} = \mathbb{I}(\kappa = \arg \max_{\kappa'} d_{n,\kappa}), \forall (n, \kappa) \in S(r)$
 $x_k = \arg \min_x \sum_{n \in [N]} r_{n,\kappa} \text{dist}_{w_k}(x, y_n)$
end while
 $l_k = \sum_{n \in [N], \kappa \in [k]} r_{n,\kappa} d_{n,\kappa}$
Output: x_k, l_k

time of M/GP-MBTL closely follows that of the algorithm it selects. Note that all reported runtimes exclude the time required for training the policies.

I Details in GP-MBTL

I.1 Gaussian Process Model-Based Transfer Learning (Cho et al. 2024)

A practical solution to solve GSTS problem is provided by MBTL (Cho et al. 2024), which we refer to as **GP-MBTL** in this work. The key idea is to separately estimate the source task performance with Gaussian Process (GP) Regression and model the generalization gap with a linear function of the context dissimilarity. Although the original MBTL formulation targets one-dimensional contexts, it can be extended to higher dimensions by using norm-based distances. Since continuous task spaces X can be large or even infinite in a multi-dimensional context space, GP-MBTL discretizes X into a finite grid, which enables applying BO methods on a manageable set of candidate source tasks.

At each iteration k , GP-MBTL selects a new source task x_k by maximizing an acquisition function. Intuitively, the algorithm favors tasks x that (i) exhibit high estimated performance $\mu_{k-1}(x)$, (ii) have high estimation uncertainty $\sigma_{k-1}(x)$, and (iii) incur a small estimated generalization gap to other tasks in Y . Concretely, an acquisition function is:

$$a(x; x_{1:k-1}) = \mathbb{E}_{y_n \in \mathcal{U}(Y)} [[\mu_{k-1}(x) + \beta_k^{1/2} \sigma_{k-1}(x) - \Delta \hat{J}(\pi_x, y_n) - \hat{J}_{k-1}(y_n)]_+], \quad (13)$$

where β_k is a user-specified exploration parameter, and $[\cdot]_+$ denotes $\max(\cdot, 0)$. $\Delta \hat{J}(\pi_x, y_n)$ models how much performance is *estimated* to be lost when transferring π_x to y_n , while $\hat{J}_{k-1}(y_n)$ represents the estimated best policy performance on y_n from previously trained source tasks. Thus, the acquisition function estimates the expected improvement from training on task x . By iterating this procedure—training a policy on the chosen source task, updating the GP estimates with the newly observed performance, and selecting the most promising next source task—GP-MBTL incrementally improves its selection of source tasks to maximize overall performance across Y .

Furthermore, we note that, in this paper, we leverage actual generalization performance when computing the acquisition

Algorithm 6: GP-MBTL

Input: Task set $Y = \{y_n\}_{n \in [N]}$.
Discretize X to \bar{X}
Initialize $J, V = 0, \forall x \in \bar{X}$
for $k \in [K]$ **do**
 if $k = 1$ **then**
 $x_1 \leftarrow \text{median}(\bar{X})$
 else
 $\mu_{k-1}, \sigma_{k-1} \leftarrow \mathcal{GP}(\mathbb{E}_{x \in x_{1:k-1}} [J(\pi_x, x)], \kappa(x, \tilde{x}))$
 Calculate $a(x; x_{1:k-1})$ with Eq. 14
 $x_k = \arg \max_x a(x; x_{1:k-1})$
 end if
 Train on x_k , get π_{x_k}
 Transfer to target tasks, receive $\{J(\pi_{x_k}, y_n)\}_{n \in [N]}$
 Calculate θ with Eq. 15
end for

function and enable online detection of the generalization gap's slope beyond the original GP-MBTL. More details are provided in Appendix I.2. However, we found that GP-MBTL is not efficient in solving all CMDP problems. In the following section, we will show how we can detect and leverage CMDP structures for training task selection.

I.2 Revised GP-MBTL

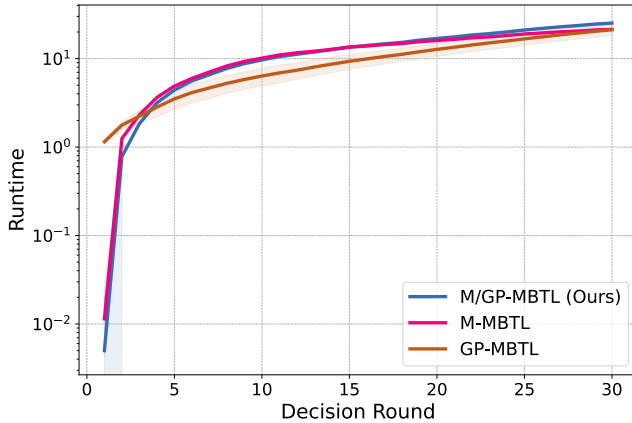
Update with Real Generalization Gaps. The original GP-MBTL (Cho et al. 2024) uses *modeled* generalization gaps despite having cheap access to *real* generalization gaps, since evaluation of a policy is much cheaper than training. Thus, in this work, we use the real generalization performance to calculate the best available performance $\max_{x' \in x_{1:k-1}} J(\pi_{x'}, y_n)$, as opposed to the estimated performance in (Cho et al. 2024). Thus, we get the acquisition function for task selection as follows:

$$a(x; x_{1:k-1}) = \mathbb{E}_{y_n \in \mathcal{U}(Y)} [[\mu_{k-1}(x) + \beta_k^{1/2} \sigma_{k-1}(x) - \Delta \hat{J}(\pi_x, y_n) - \max_{x' \in x_{1:k-1}} J(\pi_{x'}, y_n)]_+], \quad (14)$$

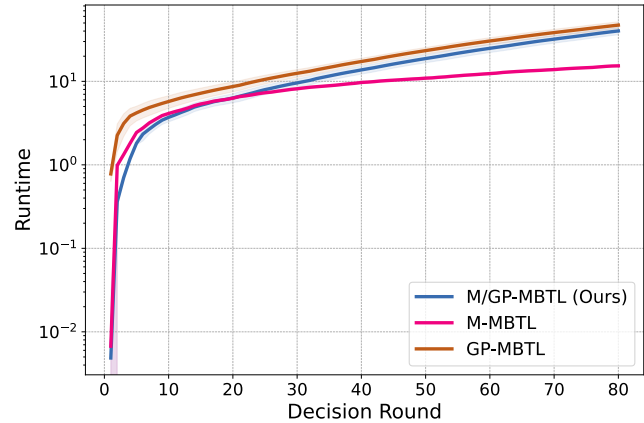
Slope Learning. The original GP-MBTL operates on a single θ value for generalization gap estimation ($\Delta J(\pi_x, y) = \theta|x - y|$, where $\theta \in \mathbb{R}^+$) under Assumption 4.2. When extending the generalization gap model to multi-dimensional cases, we may consider different slopes for different directions and different dimensions. Also, since the slopes are not necessarily positive as we discussed in Slope Criterion in Section 4.2, we consider $\theta \in \mathbb{R}$. Recall that $\text{diff}_{\kappa,n} = [[x_\kappa - y_n]_-, [x_\kappa - y_n]_+]$. Similar to Slope Criterion, we propose to use a linear relationship $\hat{J}(\pi_{x_\kappa}, y_n) = \theta^\top \text{diff}_{\kappa,n}$, and learn the slope θ by linear regression:

$$\theta = \text{Linear Regression}(\{J(\pi_\kappa, y_n)\}_{n \in [N], \kappa \in [k]}, \{\text{diff}_{\kappa,n}\}_{n \in [N], \kappa \in [k]}), \quad (15)$$

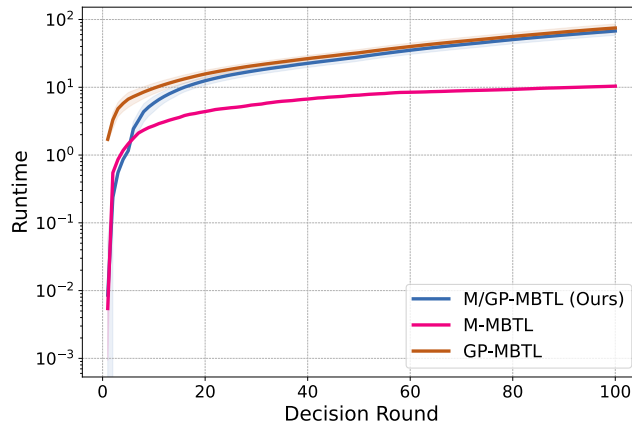
where $\pi_\kappa = \pi_{x_\kappa}$. In this way, GP-MBTL can automatically adapt to CMDP problems with varying slopes in the generalization gap of different dimensions (Algorithm 6).



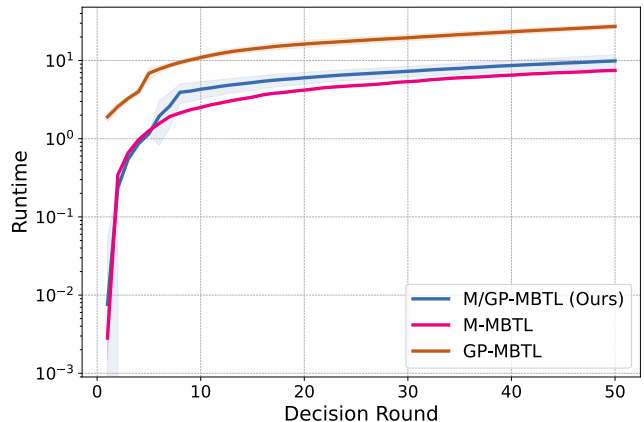
(a) CartPole



(b) BipedalWalker



(c) IntersectionZoo



(d) CyclesGym

Figure 4: CPU time comparison of M/GP-MBTL with M-MBTL and GP-MBTL on the CartPole, BipedalWalker, IntersectionZoo, and CyclesGym benchmarks.

I.3 GP library

Another modification concerns the Gaussian-process implementation in GP-MBTL. While Cho et al. (2024) relies on `GaussianProcessRegressor` from `scikit-learn`, which must be retrained from scratch at every iteration k and thus becomes a computational bottleneck as k grows, we instead adopt `gpytorch.models.ExactGP` (Gardner et al. 2018). Its neural-network parameterization of the mean and covariance enables efficient online updates, eliminating the need for full retraining at each step.

J Comparison between M-MBTL and GP-MBTL

We compare M-MBTL and GP-MBTL through the generalization-performance decomposition introduced in Definition 3.1. Under MOUNTAIN structure we set $f(x) = C_1$ and $h(x, y) = \text{dist}(x, y)$; consequently, M-MBTL needs only to estimate $g(y)$ via Eq. (3). GP-MBTL (Cho et al. 2024), by contrast, assumes a linear generalization gap $\Delta J(\pi_x, y) = J(\pi_x, x) - J(\pi_x, y) = g(x) - g(y) - h(x, y)$

which can be interpreted as a constant task difficulty $g(y) = C$ plus a linear interaction $h(x, y)$. GP-MBTL estimates the source-task performance using a Gaussian Process. With $g(y)$ constant, it is equivalent to estimating $f(x)$. However, when task difficulty is not constant, this approximation becomes inaccurate and GP-MBTL may underperform M-MBTL. However, our revised GP-MBTL (Appendix I.2) mitigates this issue by using actual generalization performance to compute the acquisition function. As a result, errors in estimating the generalization performance of trained policies do not directly affect task selection, reducing the impact of this problem. Consequently, GP-MBTL can still perform better than M-MBTL in some cases, especially when MOUNTAIN structure is violated. Thus, we use GP-MBTL as a more general solution for M/GP-MBTL when MOUNTAIN is not detected.

K Details in Structure Detection Model-Based Transfer Learning

Below, we present the details about key algorithms that form the backbone of our SD-MBTL framework. Algorithm 7 out-

lines the generic Structure Detection Model-Based Transfer Learning (SD-MBTL) framework. The input of SD-MBTL includes a task set Y , a CMDP structures set S , a detection algorithm $\text{Detect} : \mathbb{R}^{k \times N} \rightarrow S$, and MBTL algorithms $(\text{Alg}_1, \text{Alg}_2, \dots, \text{Alg}_{|S|})$. In each decision round, the algorithm first detects the underlying CMDP structure based on observed generalization performance and then uses a mapping function to select the corresponding MBTL algorithm. The chosen algorithm then selects the next training task, which is subsequently used to update the performance estimates.

Algorithm 7: SD-MBTL

Input: Task set $Y = \{y_n\}_{n \in [N]}$, CMDP structures set S , Detection algorithm Detect , MBTL algorithms $\text{Alg}_1, \text{Alg}_2, \dots, \text{Alg}_A$.

for $k \in [K]$ **do**

$s_i = \text{Detect}(\{J(\pi_\kappa, y_n)\}_{n \in [N], \kappa \in [k-1]})$

Run Alg_i corresponding to the structure s_i , get training task x_k

Train on x_k , receive $\{J(\pi_\kappa, y_n)\}_{n \in [N]}$

end for

L Oracle

L.1 Definitions

We define Myopic Oracle as an optimal myopic solution to solve the GSTS problem.

Definition L.1 (Myopic Oracle). Myopic oracle greedily selects the training task that maximizes the expected generalization performance over target task y and W trial in each step k .

$$x_k = \arg \max_{x \in X \setminus \{x_{1:k-1}\}} \frac{1}{W} \sum_{w=1}^W \mathbb{E}_{y \in \mathcal{U}(Y)} \left[\max_{x' \in x_{1:k-1} \cup \{x\}} J_{(w)}(\pi_{x'}, y) \right] \quad (16)$$

L.2 Discussion

For completeness, we provide a formal definition of the oracle introduced in (Cho et al. 2024), termed the “Sequential Oracle.” Unlike the myopic oracle, the Sequential Oracle selects a different training task for each experimental trial, as though it knew the random seed in advance—an idealized capability that is unattainable in practice.

Definition L.2 (Sequential Oracle). For each trial w , Sequential oracle greedily selects the training task x_k^w that maximizes the expected generalization performance over target task y in each step k .

$$x_k^w = \arg \max_{x \in X \setminus \{x_{1:k-1}\}} \mathbb{E}_{y \in \mathcal{U}(Y)} \left[\max_{x' \in x_{1:k-1} \cup \{x\}} J_{(w)}(\pi_{x'}, y) \right] \quad (17)$$

M Aggregated Metric

On the CMDP benchmarks, we design an aggregated performance metric, an adaptation of the widely used human-normalized score (HNS) in (Badia et al. 2020) and (Mnih

et al. 2015). This helps us evaluate how baseline algorithms perform across multiple benchmarks—particularly suited for MBTL-based methods. For each benchmark, we calculate an algorithm’s performance by subtracting the Random baseline and then dividing by the difference between the Myopic Oracle’s performance and the Random baseline. This yields a normalized performance. Formally,

$$\text{Normalized Performance}_j = \frac{\text{Performance}_j - \text{Random}_j}{\text{Myopic Oracle}_j - \text{Random}_j}, \quad (18)$$

where the subscription j represents the performance at benchmark j . We then average an algorithm’s normalized performance across the four benchmarks to obtain its aggregated performance, as recommended by (Agarwal et al. 2021a):

$$\text{Aggregated Performance} = \sum_j \text{Normalized Performance}_j \quad (19)$$

Under this metric, a value of 0 represents the performance of the Random baseline, while a value of 1 represents the performance of the Myopic Oracle. This metric scales each MBTL-based algorithm’s score between 0 and 1, indicating how much it outperforms the Random baseline and how closely it approaches the Myopic Oracle.

N Implementation Details

N.1 Construction of transfer matrix.

For the ease of our analysis, we first construct the transfer matrix. To do so, we first train each task in the discrete task set independently. This provides the policies trained on all source tasks, making it easier to compare the performance of different algorithms in source task selection. Based on the average performance after the transfer, we construct a transfer matrix. The transfer matrix is an $N \times N$ matrix, where the element at the i -th row and j -th column represents the generalization performance of policy trained from i -th task and applied to j -th task. This also allows us to try many different types of multi-policy training algorithms that can layer on top of any DRL algorithm with the low cost of training. The above experiments were repeated three times.

N.2 Benchmarks

CartPole For the CartPole task, we employ the default environment context variables provided by the CARL library (Benjamins et al. 2023): a pole length of 0.5, a cart mass of 1.0, and a pole mass of 0.1. To generate three-dimensional context variations, each variable was varied over a range from 0.2 to 2 times its default value, resulting in $N = 9 \times 10 \times 10$ unique contexts. Each independent training run is conducted for five million simulation timesteps.

BipedalWalker For the BipedalWalker CMDP, we similarly modify the environment using the CARL library. In this benchmark, we vary three context variables—friction, gravity, and scale—over a range from 0.2 to 1.6 times their default values, yielding $N = 8 \times 8 \times 8$ distinct tasks. The default settings for BipedalWalker are a friction value of 2.5, a scale

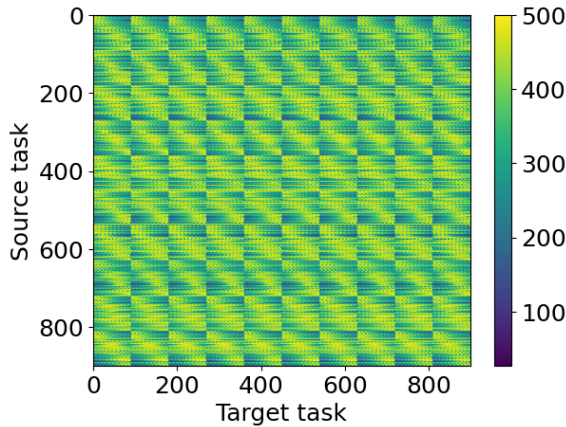


Figure 5: Transfer matrices of three context variables in the CartPole task (pole length, cart mass, pole mass). Brighter colors indicate higher generalization performance.

of 30, and a gravity of 10. As with CartPole, each independent training run is executed for five million time steps, and the best-performing model is selected for zero-shot transfer evaluation.

CARL benchmarks are distributed under the Apache License 2.0.

IntersectionZoo For the IntersectionZoo benchmark, we configure the simulation with a default inflow of 250 vehicles per hour, an autonomous vehicle penetration rate of 0.5, and a green phase duration of 20 seconds to replicate realistic urban traffic conditions. The CMDP context variables vary from 0.1 to 1.2 times their default values, resulting in a total of 6^3 distinct contexts. We employ version 1.16.0 of the microscopic traffic simulator, Simulation of Urban MObility (SUMO) (Lopez et al. 2018) v.1.16.0. For further details on the experimental setup and hyperparameter configurations, please refer to (Jayawardana et al. 2025). The IntersectionZoo benchmark falls under the MIT License.

CyclesGym For CyclesGym benchmark (Turchetta et al. 2022), we start with default environmental context variables that simulate realistic agricultural conditions—specifically, a default precipitation of 10.0, a temperature of 20.0, and a sunlight (solar) intensity of 15.0. To generate a diverse set of contexts, we independently scale each of these context variables using scaling factors drawn from a predefined list (e.g., 0.5, 1.0, 1.5, 2.0, 2.5, 3.0), forming a three-dimensional grid of contexts (amounting to 6^3 combinations). These context variables are set up to evaluate our method’s performance thoroughly across various simulated agricultural scenarios. Each trial is run three times (using seeds 0, 1, and 2) to ensure robustness under fixed weather and non-adaptive settings. CyclesGym benchmark falls under the BSD 3-Clause License.

Detailed context variables and their ranges are listed in Table 4.

N.3 Synthetic Data

Transfer matrices. To systematically evaluate transfer performance across controlled task variations, we generate a family of 512 “synthetic” tasks. Each task is defined by a 3-dimensional integer context vector $x \in \{1, \dots, 8\}^3$. In Figure 13, each subplot visualizes a 512x512 matrix whose (i, j) entry is the average performance $J(\pi_{x_i}, x_j)$. Bright cells indicate high performance and dark cells indicate low performance. By comparing across panels, one can clearly see the effect of adding linear source ($f(x)$), target ($g(y)$) biases, and different interaction term $h(x, y)$ can produce structured transfer matrices, and how noise induces realistic transfer matrices.

N.4 Deep RL Training

We employ the PPO implementation from the stable-baselines3 library (Raffin et al. 2021) for our deep reinforcement learning experiments. All training runs are executed on a distributed computing cluster featuring Intel(R) Xeon(R) CPU E5-2670 v2 @ 2.50GHz, with each independent training run utilizing four CPUs. Multi-task training is concurrently exposed to all target CMDPs, and the training is halted once the training convergence is achieved.

N.5 Hyperparameters

Random Seeds We test the algorithms with 100 bootstrapped transfer matrices. For the random selection algorithm, we take the average of 50 repeats for each transfer matrix, whereas other algorithms were repeated only once. For transfer matrix w and repeat j , we use random seed $(w + 1) \times (j + 1)$.

M-MBTL M-MBTL uses the L_1 norm distance with slope 0.01 in each dimension. We choose L_1 norm distance because we assume that the influence of different context dimensions is independent. Since we normalize the generalization performance to the range 0–1, choosing a fixed slope of 0.01 is a relatively moderate option. We assign the same slope to every dimension because we have no prior information about differences between dimensions; therefore, we assume that each dimension exerts an equal level of influence. Since the number of tasks is relatively small, and the clustering process for each candidate takes a shorter time, we use the number of samples $M = N$.

GP-MBTL GP-MBTL also uses L_1 norm distance with slope 0.01 in each dimension. We used `gpytorch.kernels.RBFKernel` in (Gardner et al. 2018) with default hyperparameters as the kernel function for the Gaussian Process.

RL Training Table 5 lists the RL-training hyperparameters for CartPole, BipedalWalker, IntersectionZoo, and CyclesGym benchmarks. For CartPole and BipedalWalker, we employ PPO from `stable_baselines3` (Raffin et al. 2021) with default hyperparameters, including a learning rate of 3×10^{-4} , `n_steps=2048`, batch size 64, discount factor 0.99, GAE parameter 0.95, clipping parameter 0.2, entropy coefficient 0, and a value function loss coefficient 0.5.

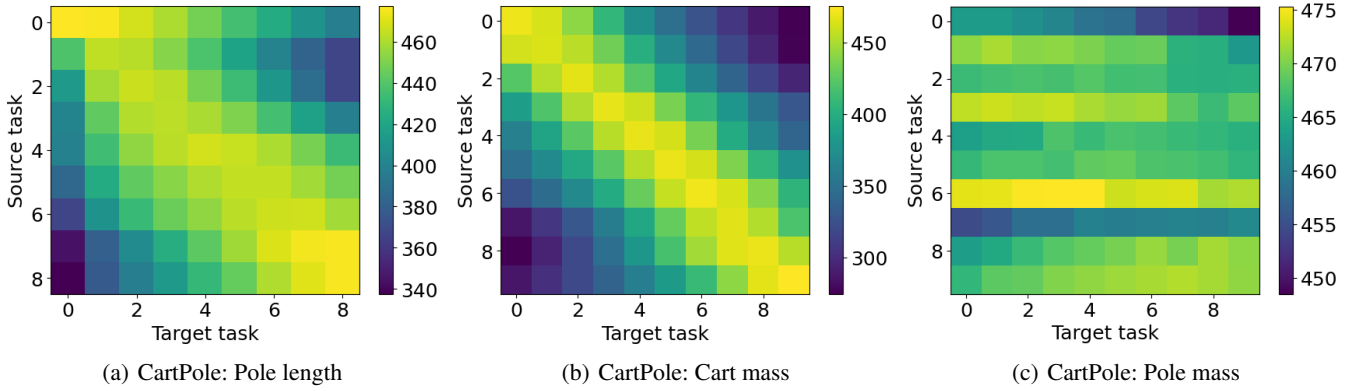


Figure 6: Average transfer matrices of three context variables in the CartPole task (pole length, cart mass, pole mass). The average transfer matrix is computed as the average of local transfer matrices, where each local transfer matrix varies only one variable while keeping the other two variables constant. Brighter colors indicate higher generalization performance.

Table 4: Environmental context variables for each benchmark.

Benchmark	Variable	Default	Variation Range	# Values
CartPole	Pole length	0.5	0.4 - 2.0 x default	9
	Cart mass	1.0	0.2 - 2.0 x default	10
	Pole mass	0.1	0.2 - 2.0 x default	10
BipedalWalker	Friction	2.5	0.2 - 1.6 x default	8
	Scale	30	0.2 - 1.6 x default	8
	Gravity	10	0.2 - 1.6 x default	8
IntersectionZoo	Inflow rate	250 veh/h	0.1 - 1.2 x default	6
	AV penetration rate	0.5	0.1 - 1.2 x default	6
	Green-phase duration	20 s	0.1 - 1.2 x default	6
CyclesGym	Precipitation	10.0	{0.5, 1.0, 1.5, 2.0, 2.5, 3.0} x default	6
	Temperature	20.0	{0.75, 1.0, 1.25, 1.5, 1.75, 2.0} x default	6
	Sunlight	15.0	{0.5, 1.0, 1.5, 2.0, 2.5, 3.0} x default	6

For IntersectionZoo, we configure PPO with a policy clip of 0.03 and began with a KL-divergence penalty coefficient of 0.1, aiming to maintain KL-divergence around 0.02 throughout training. The value network employ a clipping threshold of ± 3 and carried a loss weight of 1. To foster exploration, we add an entropy bonus weighted at 0.005. Each epoch comprises 10 gradient-update steps, and the model is trained for 5,000 epochs, running 10 episodes per epoch. Episodes last up to 1,500 time steps, and we sample mini-batches of 40 transitions. Optimization is handled by Adam with a learning rate of $1e-4$, weight decay of 0.97, and β -parameters (0.9, 0.999). Our policy and value networks each feature four hidden layers of 256 units, use tanh activations, and are initialized orthogonally. The simulator warm up for 50 steps before each episode, proceed with a 0.5-second step size, and we discount future rewards by $\gamma = 0.99$.

For the CyclesGym experiments, we also run PPO for a total of 20,000 time steps, evaluating performance every 1,000 steps. Each update collects 80 environment steps per rollout, with mini-batches of 64 samples and 10 optimization epochs

per update. For the others, we use the default parameters from `stable_baselines3` (Raffin et al. 2021).

O Results in Detail

O.1 Synthetic Data with Different Noise Terms

We also test our approaches on synthetic data with different noise terms. Table 6 presents the performance comparison for $\epsilon = 0$, showing results similar to those in Table 1. Table 7 presents the performance comparison for $\epsilon \sim \mathcal{N}(0, 30^2)$. With significantly increased noise, Assumptions 4.1 and 4.2 are violated to some extent in all cases, causing the CMDP structure to deviate from Mountain. Since GP-MBTL uses real generalization performance to compute the acquisition function, it demonstrates greater robustness to noise. GP-MBTL generally performs better when $g(y)$ is constant, whereas M-MBTL is more effective when $g(y)$ is linear. M/GP-MBTL consistently achieves the highest or near-highest performance, highlighting the effectiveness of structure detection in efficiently solving CMDPs with varying structural properties.

Table 5: RL-training hyperparameters for CartPole, BipedalWalker, IntersectionZoo, and CyclesGym benchmarks.

Hyperparameter	CartPole	BipedalWalker	IntersectionZoo	CyclesGym
Training steps (independent)	5×10^6	5×10^6	5×10^6	2×10^3
Training steps (multi-task)	5×10^8	7×10^8	5×10^8	4×10^4
Test episodes (train)	10	10	10	10
Evaluation episodes (transfer)	100	100	100	100

Table 6: Performance comparison on Synthetic Data ($\epsilon = 0$) with K=50.

$f(x)$	$g(y)$	$h(x, y)$	Random	GP-MBTL	M-MBTL (Ours)	M/GP-MBTL (Ours)	Myopic Oracle
Constant	Linear	Non-distance	0.7028 ± 0.0010	0.7250 ± 0.0000	0.7055 ± 0.0000	0.7250 ± 0.0000	0.7250 ± 0.0000
Constant	Linear	L_1 norm	0.7122 ± 0.0002	0.7110 ± 0.0000	0.7187 ± 0.0000	0.7187 ± 0.0000	0.7190 ± 0.0000
Constant	None	Non-distance	0.8688 ± 0.0019	0.9091 ± 0.0000	0.8736 ± 0.0000	0.9091 ± 0.0000	0.9091 ± 0.0000
Constant	None	L_1 norm	0.9244 ± 0.0005	0.9364 ± 0.0000	0.9374 ± 0.0000	0.9374 ± 0.0000	0.9382 ± 0.0000
Linear	Linear	Non-distance	0.5544 ± 0.0022	0.5714 ± 0.0000	0.5552 ± 0.0000	0.5714 ± 0.0000	0.5714 ± 0.0000
Linear	Linear	L_1 norm	0.5517 ± 0.0027	0.5714 ± 0.0000	0.5535 ± 0.0000	0.5714 ± 0.0000	0.5714 ± 0.0000
Linear	None	Non-distance	0.6761 ± 0.0032	0.7000 ± 0.0000	0.6772 ± 0.0000	0.7000 ± 0.0000	0.7000 ± 0.0000
Linear	None	L_1 norm	0.7660 ± 0.0028	0.7857 ± 0.0000	0.7678 ± 0.0000	0.7857 ± 0.0000	0.7857 ± 0.0000
Aggregated Performance			-0.0000 ± 0.0353	0.8368 ± 0.0268	0.3010 ± 0.0264	0.9873 ± 0.0015	1.0000 ± 0.0000

* Note: Values are reported as the mean performance \pm half the width of the 95% confidence interval. Rows shaded in light gray indicate the synthetic settings that satisfy our proposed MOUNTAIN structure assumption. Bold values represent the highest value(s) within the statistically significant range for each task, excluding the oracle.

Table 7: Performance comparison on Synthetic Data ($\epsilon = \mathcal{N}(0, 30^2)$) with K=50.

$f(x)$	$g(y)$	$h(x, y)$	Random	GP-MBTL	M-MBTL (Ours)	M/GP-MBTL (Ours)	Myopic Oracle
Constant	Linear	Non-distance	0.7083 ± 0.0005	0.7274 ± 0.0008	0.7091 ± 0.0003	0.7202 ± 0.0012	0.7319 ± 0.0003
Constant	Linear	L_1 norm	0.6879 ± 0.0003	0.6825 ± 0.0008	0.6879 ± 0.0003	0.6876 ± 0.0005	0.6952 ± 0.0003
Constant	None	Non-distance	0.7036 ± 0.0006	0.7274 ± 0.0006	0.7045 ± 0.0004	0.7215 ± 0.0012	0.7295 ± 0.0003
Constant	None	L_1 norm	0.7125 ± 0.0004	0.7181 ± 0.0006	0.7125 ± 0.0004	0.7150 ± 0.0006	0.7205 ± 0.0004
Linear	Linear	Non-distance	0.6815 ± 0.0008	0.6790 ± 0.0044	0.6818 ± 0.0003	0.6912 ± 0.0024	0.7135 ± 0.0003
Linear	Linear	L_1 norm	0.6840 ± 0.0010	0.6810 ± 0.0062	0.6844 ± 0.0003	0.6953 ± 0.0037	0.7234 ± 0.0003
Linear	None	Non-distance	0.7240 ± 0.0008	0.7202 ± 0.0035	0.7244 ± 0.0003	0.7272 ± 0.0024	0.7586 ± 0.0003
Linear	None	L_1 norm	0.7246 ± 0.0010	0.7366 ± 0.0028	0.7250 ± 0.0003	0.7393 ± 0.0023	0.7670 ± 0.0003
Aggregated Performance			-0.0000 ± 0.0108	0.2127 ± 0.0514	0.0147 ± 0.0089	0.3099 ± 0.0281	1.0000 ± 0.0082

* Note: Values are reported as the mean performance \pm half the width of the 95% confidence interval. Rows shaded in light gray indicate the synthetic settings that satisfy our proposed MOUNTAIN structure assumption. Bold values represent the highest value(s) within the statistically significant range for each task, excluding the oracle.

Figure 14 shows, for each of the eight synthetic CMDP configurations (varying $f(x)$, $g(y)$, and $h(x, y)$), which sub-algorithm was chosen over 100 trials and 50 rounds ($K = 50$). Red entries indicate rounds where M-MBTL was deployed; blue where GP-MBTL was deployed. In the two MOUNTAIN settings (constant f , L_1 -norm h , regardless of g), M-MBTL dominates almost every round. In all non-mountain settings (either non-distance h or non-constant f), GP-MBTL is usually selected. This confirms that our online detector correctly identifies the underlying structure and switches to the appropriate task-selection strategy in each case. Figure 15 also shows the progression of the normalized performance of our proposed M/GP-MBTL algorithm compared with various baselines in terms of decision rounds. M/GP-MBTL achieves the best—or nearly the best—performance, successfully detecting whether a CMDP satisfies MOUNTAIN structure and choosing the appropriate algorithm accordingly.

Figure 16 shows how the aggregated metric varies with K

on the 3D synthetic dataset. As K increases, the performance of M/GP-MBTL improves rapidly, surpassing GP-MBTL at around ($K = 12$), and then continues to maintain the best performance thereafter.

O.2 CMDP Benchmarks

Figure 17 shows the number of source-trained policies required to achieve ϵ -suboptimal generalization performance in CMDP benchmarks. Figure 17(a) shows that M-MBTL outperforms GP-MBTL in the early stage but is eventually caught up by GP-MBTL. The reason is that, early on, the Gaussian Process in GP-MBTL is trained on only a small amount of data, while M-MBTL makes more reliable training-task selections by leveraging the clustering loss. As the number of decision rounds grows, the prediction of the Gaussian Process becomes progressively more accurate.

In Figure 18, we present the normalized performance of

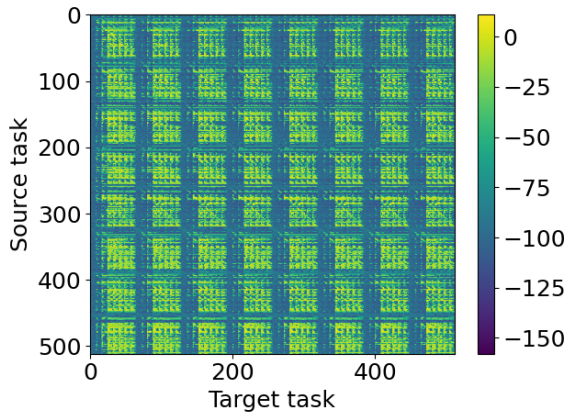


Figure 7: Transfer matrices of three context variables in the Bipedal Walker task (gravity, scale, friction). Brighter colors indicate higher generalization performance.

our proposed M/GP-MBTL algorithm compared with various baselines (including Independent Training, Multi-task Training, Stochastic Oracle, Random, and GP-MBTL) across four CMDP benchmarks in terms of decision rounds. These results demonstrate that our M/GP-MBTL approach performs almost as well as the best of M-MBTL and GP-MBTL, and approaches the myopic oracle quickly across all benchmarks.

Figure 19 also provides a detailed performance analysis using three different statistical measures: median, Interquartile Mean (IQM), and mean performance. IQM, which is robust to outliers as validated by (Agarwal et al. 2021b), serves as a reliable metric to compare the consistency of performance across different methods. These figures illustrate that M/GP-MBTL not only delivers high overall performance but also exhibits lower variability across experiment trials and benchmarks.

Table 8 presents a comparison of area under the curve (AUC) performance. AUC measures the average performance in K decision rounds, and highlights how quickly the performance of each algorithm improves. M/GP-MBTL consistently achieves the highest or near-highest AUC performance across all benchmarks. It achieves better performance than multi-task training in the CartPole benchmark, since multi-task training performs worse when the number of training steps is small. However, the AUC performance shows a larger standard deviation because the performance of each algorithm fluctuates more when k is small, especially for the random algorithm. Consequently, the performance of several algorithms may all fall within the statistically significant range.

In Figure 20, we visualize, for each of 100 independent trials and over 80 decision rounds ($K = 80$), which sub-algorithm our detector chose at each step: red entries mark rounds where M-MBTL was used, and blue entries mark GP-MBTL. As expected, in CartPole and CyclesGym CMDP, which both exhibit strong MOUNTAIN structure, M-MBTL dominates almost all rounds; in IntersectionZoo, which violates MOUNTAIN, GP-MBTL is selected nearly through-

out; and in BipedalWalker, where the structure only partially holds, the detector switches dynamically, reflecting a mixture of both strategies. This confirms that our online structure detector is correctly steering the algorithm towards the most appropriate source-task selection method in each setting.

Figure 21 shows how the aggregated metric varies with K on benchmark dataset. Different benchmarks require different values of K for the algorithms to converge to stable performance. Classic control tasks such as Cartpole and Walker converge with relatively small K , whereas IntersectionZoo and CyclesGym require much larger K . Therefore, we group the four benchmarks into two sets and plot the aggregated metric curves separately. Figure 21(a) shows the aggregated metrics for Cartpole and Walker, where M/GP-MBTL relies mainly on M-MBTL, resulting in similar performance between the two. Figure 21(b) shows the aggregated metrics for IntersectionZoo and CyclesGym, where the performance of M/GP-MBTL rises rapidly after around $K = 7$ and surpasses the other baselines.

O.3 Abalation Study

To verify the effectiveness of individual algorithms and the online structure detection module in M/GP-MBTL, we compare M/GP-MBTL against standalone M-MBTL, standalone GP-MBTL, and two hybrid baselines that each combine an algorithm with a random policy. M-MBTL+Random uses M-MBTL only when the Mountain structure is detected, and GP-MBTL+Random applies GP-MBTL only when its linear-gap assumption holds. In all other cases, they are reverted to random selection.

Figure 22 shows the ablation study results. In CartPole, BipedalWalker, and CyclesGym, M-MBTL+Random performs nearly as well as M/GP-MBTL because those tasks largely satisfy Mountain structure. Across BipedalWalker, CyclesGym, and IntersectionZoo, M/GP-MBTL consistently outperforms GP-MBTL+Random, and it also exceeds M-MBTL+Random on IntersectionZoo. These results demonstrate that combining M-MBTL and GP-MBTL enables the framework to leverage the strengths of both methods, and that M/GP-MBTL selects the appropriate algorithm under various CMDP structures.

O.4 Performance Distribution: Real vs. Bootstrapped Data

Due to the substantial computational resources required to independently train each CMDP, we were limited to only three trials per task. Even these three trials took several months to complete. To address this limitation—and leveraging the fact that each context-MDP training is independent—we generated 97 bootstrapped datasets by combining the available trials in different ways. For the construction of the transfer matrix, each row (representing a source task) was randomly selected from one of the three available training runs. Consequently, the rows of the matrix may originate from different combinations of these trials.

Figure 23 presents histograms that compare M/GP-MBTL performance. This comparison is drawn between performance achieved using the original, limited real DRL data

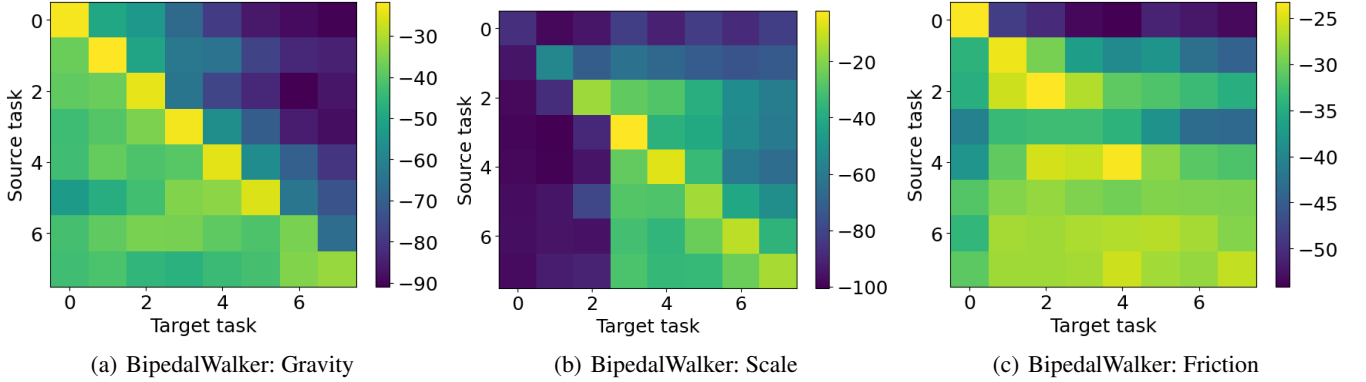


Figure 8: Average transfer matrices of three context variables in the Bipedal Walker task (gravity, scale, friction). The average transfer matrix is computed as the average of local transfer matrices, where each local transfer matrix varies only one variable while keeping the other two variables constant. Brighter colors indicate higher generalization performance.

Table 8: Performance comparison of different methods on CMDP benchmarks

Benchmark (CMDP)	Independent	Multi-task	Random	GP-MBTL	M-MBTL (Ours)	M/GP-MBTL (Ours)	Myopic Oracle
CartPole ($K = 12$)	0.9346 ± 0.0003	0.9246 ± 0.0393	0.9502 ± 0.0046	0.9542 ± 0.0069	0.9612 ± 0.0056	0.9612 ± 0.0056	0.9939 ± 0.0005
BipedalWalker ($K = 12$)	0.7794 ± 0.0011	0.5680 ± 0.0919	0.7482 ± 0.0061	0.7735 ± 0.0043	0.7800 ± 0.0020	0.7788 ± 0.0019	0.8383 ± 0.0015
IntersectionZoo ($K = 50$)	0.2045 ± 0.0008	0.3788 ± 0.1059	0.4580 ± 0.0107	0.4824 ± 0.0093	0.4183 ± 0.0040	0.4626 ± 0.0066	0.6238 ± 0.0087
CyclesGym ($K = 50$)	0.2133 ± 0.0002	0.2081 ± 0.0002	0.2119 ± 0.0009	0.2138 ± 0.0002	0.2141 ± 0.0002	0.2143 ± 0.0002	0.2181 ± 0.0001
Aggregated Performance	-0.5824 ± 0.0796	-1.3987 ± 0.6393	0.0000 ± 0.0432	0.1494 ± 0.0471	0.1472 ± 0.0412	0.2198 ± 0.0364	1.0000 ± 0.0155

* Note: Values are reported as the mean performance \pm half the width of the 95% confidence interval. Bold values represent the highest value(s) within the statistically significant range for each task, excluding the oracle.

and performance derived from the 97 bootstrapped datasets, across four distinct CMDP benchmarks: CartPole, BipedalWalker, CyclesGym, and IntersectionZoo. The results depicted in the figure demonstrate a consistency between the performance distributions obtained from the bootstrapped data and the discrete performance points observed from the real trials. The bootstrapping process generates a more continuous spectrum of performance values. Crucially, the denser regions within these bootstrapped distributions generally align well with the specific performance levels indicated by the sparse real data.

0.5 Higher Dimensional Experiments

Tables 9 and 10 report the performance comparison between M/GP-MBTL and other baselines under 5-dimensional and 7-dimensional context settings.

In the 5-dimensional experiments, we use a linear function $f(x) = [2, 2, 2, 2, 2] \cdot x$ and $g(y) = [2, 2, 2, 2, 2] \cdot y$ for non-constant case, and $f(x) = 0, g(y) = 0$ for constant case. When distance metric holds, $h(x, y) = -[3, 3, 3, 3, 3] \cdot |x - y|$. We test two non-distance cases. In case 1, $h(x, y) = -([3, 3, 3, 3, 3] \cdot [x - y]_+ + [1, 1, 1, -3, -3] \cdot [x - y]_-)$. In

case 2, $h(x, y) = -([3, 3, 3, 3, 3] \cdot [x - y]_+ + [1, 1, 1, 1, -3] \cdot [x - y]_-)$.

Since testing in high-dimensional settings typically requires substantial computation time, in the 7-dimensional experiments we only tested the four cases regarding whether $g(y)$ is constant and whether $h(x, y)$ satisfies the properties of a distance metric. We use a linear function $g(y) = [2, 2, 2, 2, 2, 2, 2] \cdot y$ for non-constant case, and $g(y) = 0$ for constant case. When distance metric holds, $h(x, y) = -[3, 3, 3, 3, 3, 3, 3] \cdot |x - y|$. Otherwise, $h(x, y) = -([3, 3, 3, 3, 3, 3, 3] \cdot [x - y]_+ + [1, 1, 1, 1, 1, -3, -3] \cdot [x - y]_-)$.

In both the 5-dimensional and 7-dimensional experiments, M/GP-MBTL demonstrated the best overall performance with relatively small confidence intervals, indicating greater robustness. In contrast, GP-MBTL showed much larger confidence intervals, reflecting its instability across different CMDP structures.

Table 9: Performance comparison on 5D Synthetic Data ($\epsilon = \mathcal{N}(0, 5^2)$) with K=50.

$f(x)$	$g(y)$	$h(x, y)$	Random	GP-MBTL	M-MBTL	M/GP-MBTL (Ours)	Myopic Oracle
Linear	Linear	L_1 norm	0.5996 ± 0.0039	0.6229 ± 0.0003	0.5993 ± 0.0010	0.6122 ± 0.0091	0.6265 ± 0.0002
Linear	Linear	Non-distance 1	0.6142 ± 0.0012	0.6120 ± 0.0022	0.6156 ± 0.0002	0.6160 ± 0.0006	0.6236 ± 0.0004
Linear	Linear	Non-distance 2	0.6128 ± 0.0018	0.6140 ± 0.0020	0.6142 ± 0.0005	0.6172 ± 0.0008	0.6262 ± 0.0005
Linear	Constant	L_1 norm	0.7348 ± 0.0040	0.7440 ± 0.0071	0.7344 ± 0.0011	0.7461 ± 0.0061	0.7626 ± 0.0002
Linear	Constant	Non-distance 1	0.6891 ± 0.0016	0.6810 ± 0.0060	0.6910 ± 0.0003	0.6910 ± 0.0010	0.7016 ± 0.0005
Linear	Constant	Non-distance 2	0.7007 ± 0.0023	0.6930 ± 0.0076	0.7024 ± 0.0006	0.7012 ± 0.0031	0.7175 ± 0.0006
Constant	Linear	L_1 norm	0.7049 ± 0.0006	0.6887 ± 0.0089	0.7090 ± 0.0004	0.7089 ± 0.0003	0.7117 ± 0.0004
Constant	Linear	Non-distance 1	0.6982 ± 0.0068	0.7463 ± 0.0006	0.6917 ± 0.0019	0.7421 ± 0.0014	0.7482 ± 0.0002
Constant	Linear	Non-distance 2	0.7000 ± 0.0027	0.7457 ± 0.0021	0.6987 ± 0.0015	0.7441 ± 0.0017	0.7503 ± 0.0001
Constant	Constant	L_1 norm	0.7374 ± 0.0007	0.7411 ± 0.0010	0.7423 ± 0.0005	0.7422 ± 0.0004	0.7457 ± 0.0005
Constant	Constant	Non-distance 1	0.7482 ± 0.0089	0.8134 ± 0.0012	0.7396 ± 0.0026	0.8129 ± 0.0002	0.8150 ± 0.0003
Constant	Constant	Non-distance 2	0.7548 ± 0.0035	0.8189 ± 0.0002	0.7531 ± 0.0020	0.8167 ± 0.0008	0.8202 ± 0.0001
Aggregated Performance			0.0000 ± 0.0356	0.1528 ± 0.2728	0.1124 ± 0.0602	0.5327 ± 0.0906	1.0000 ± 0.0090

* Note: Values are reported as the mean performance \pm half the width of the 95% confidence interval. Rows shaded in light gray indicate the synthetic settings that satisfy our proposed MOUNTAIN structure assumption. Bold values represent the highest value(s) within the statistically significant range for each task, excluding the oracle.

Table 10: Performance comparison on 7D Synthetic Data ($\epsilon = \mathcal{N}(0, 5^2)$) with K=50.

$f(x)$	$g(y)$	$h(x, y)$	Random	GP-MBTL	M-MBTL	M/GP-MBTL (Ours)	Myopic Oracle
Constant	Constant	L_1 norm	0.7136 ± 0.0002	0.7171 ± 0.0013	0.7199 ± 0.0002	0.7191 ± 0.0013	0.7239 ± 0.0001
Constant	Constant	Non-distance	0.7395 ± 0.0001	0.8151 ± 0.0009	0.7308 ± 0.0002	0.8139 ± 0.0003	0.8172 ± 0.0001
Constant	Linear	L_1 norm	0.6845 ± 0.0001	0.6786 ± 0.0025	0.6895 ± 0.0002	0.6895 ± 0.0002	0.6928 ± 0.0001
Constant	Linear	Non-distance	0.6948 ± 0.0001	0.7466 ± 0.0051	0.6881 ± 0.0001	0.7435 ± 0.0046	0.7548 ± 0.0001
Aggregated Performance			-0.0000 ± 0.0051	0.3625 ± 0.3053	0.2473 ± 0.1465	0.7270 ± 0.0811	1.0000 ± 0.0032

* Note: Values are reported as the mean performance \pm half the width of the 95% confidence interval. Rows shaded in light gray indicate the synthetic settings that satisfy our proposed MOUNTAIN structure assumption. Bold values represent the highest value(s) within the statistically significant range for each task, excluding the oracle.

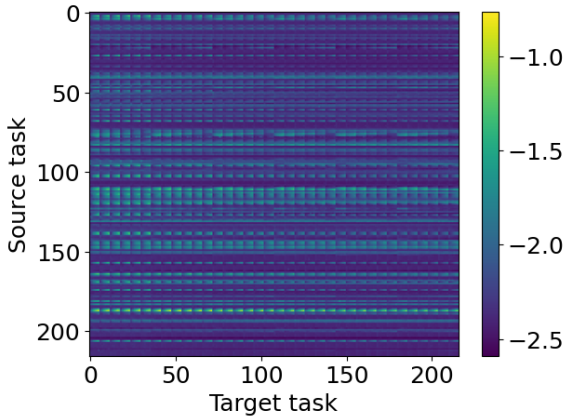


Figure 9: Transfer matrices of three context variables in the IntersectionZoo task (inflow rate, autonomous vehicle (AV) penetration rate, signal green-phase duration). Brighter colors indicate higher generalization performance.

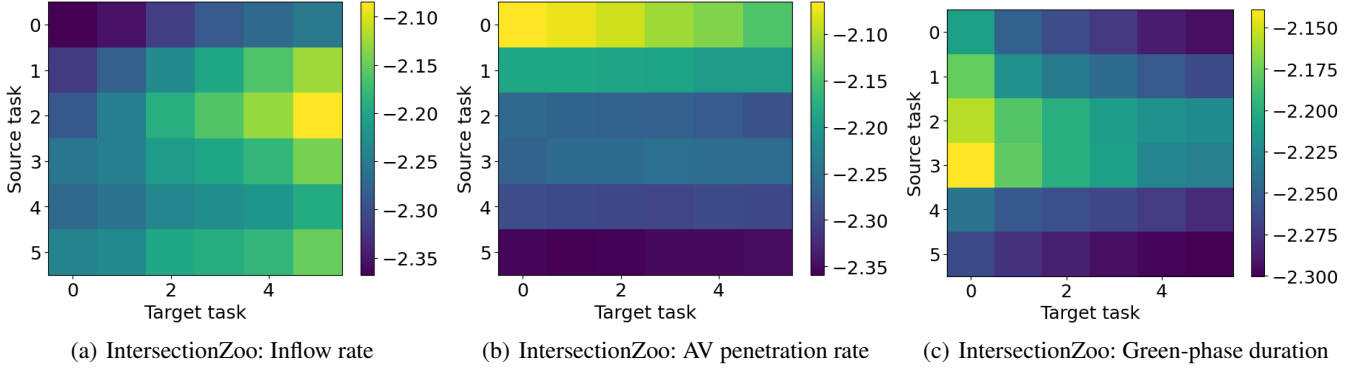


Figure 10: Average transfer matrices of three context variables in the IntersectionZoo task (inflow rate, autonomous vehicle (AV) penetration rate, signal green-phase duration). The average transfer matrix is computed as the average of local transfer matrices, where in each local transfer matrix, only one variable is changed while the other two variables are kept constant. Brighter colors indicate higher generalization performance.

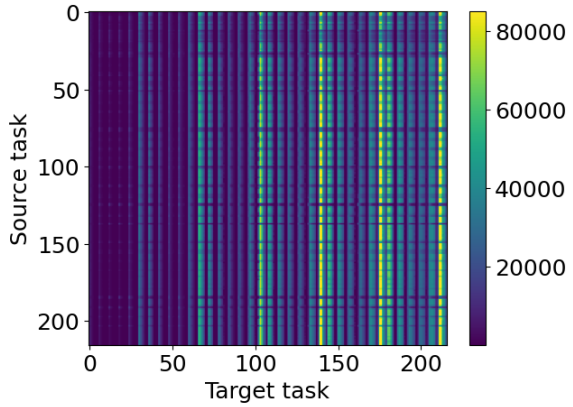


Figure 11: Transfer matrices of three context variables in the CyclesGym (precipitation, temperature, sunlight). Brighter colors indicate higher generalization performance.

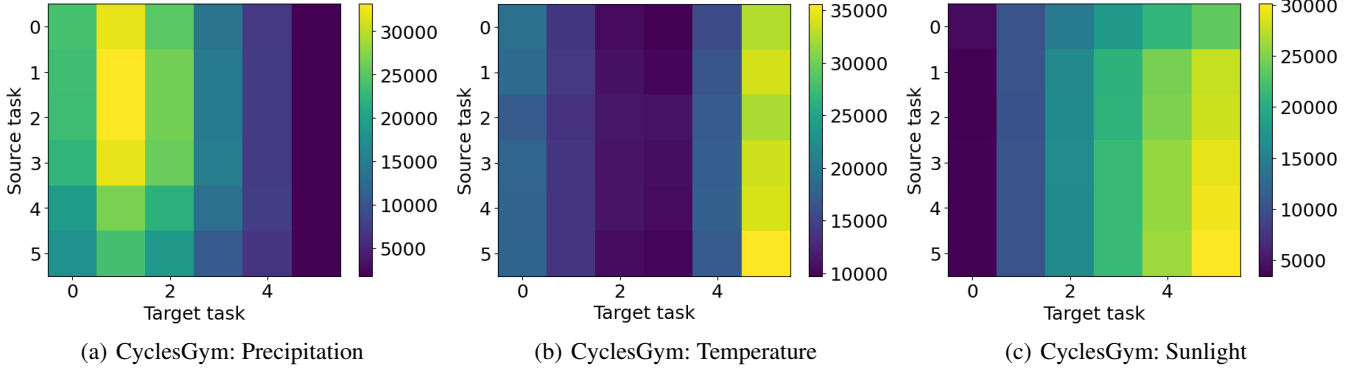


Figure 12: Average transfer matrices of three context variables in the CyclesGym (precipitation, temperature, sunlight). The average transfer matrix is computed as the average of local transfer matrices, where each local transfer matrix varies only one variable while keeping the other two variables constant. Brighter colors indicate higher generalization performance.

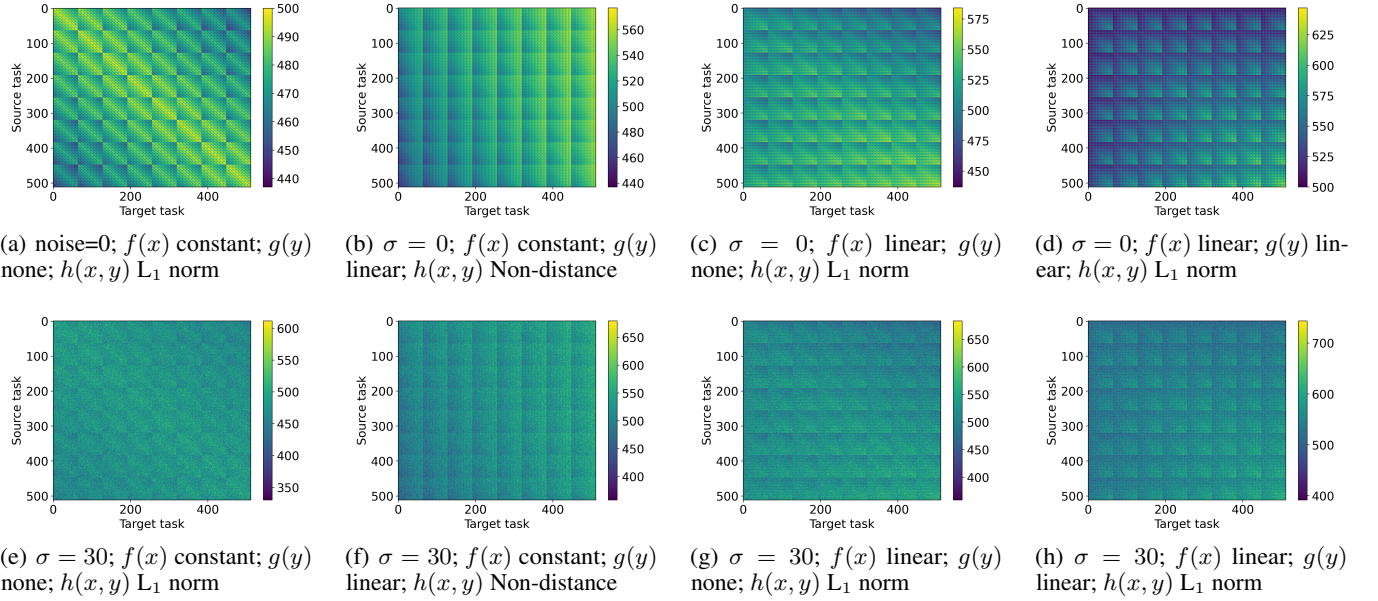


Figure 13: Transfer matrices of synthetic data with different configurations. Brighter colors indicate higher generalization performance.

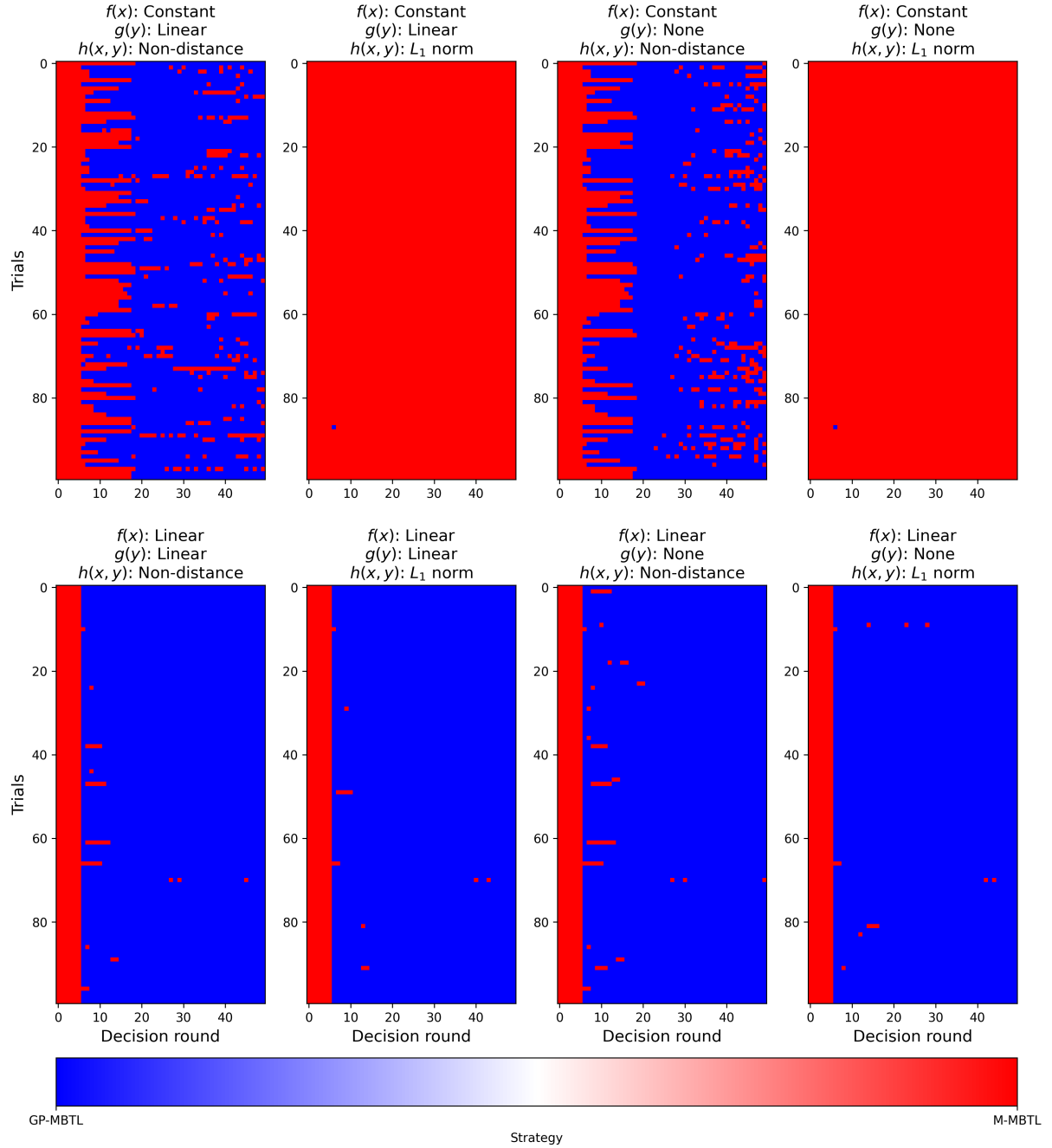


Figure 14: Per-round algorithm choice over 100 trials ($K = 50$) for eight synthetic CMDP configurations with $\epsilon \sim \mathcal{N}(0, 5^2)$. **Red** = M-MBTL; **blue** = GP-MBTL. Only the data with MOUNTAIN structure (constant $f(x)$, L_1 -norm $h(x, y)$) consistently trigger M-MBTL; all others default to GP-MBTL.

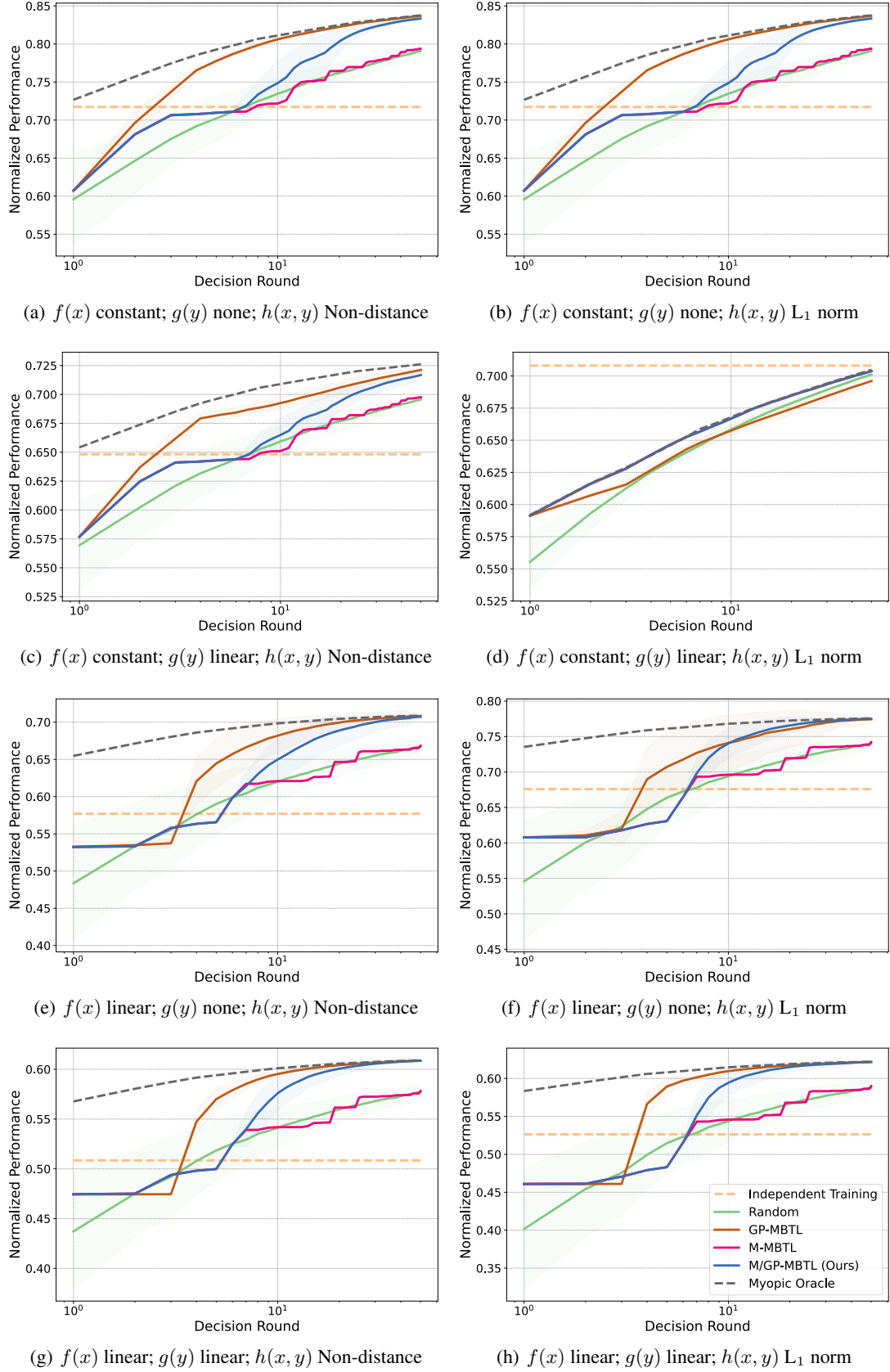


Figure 15: Normalized performance comparison of M/GP-MBTL with other baselines (Independent Training, Stochastic Oracle, Random, and MBTL baselines) on the synthetic data ($\epsilon \sim \mathcal{N}(0, 5^2)$) with $K = 50$.

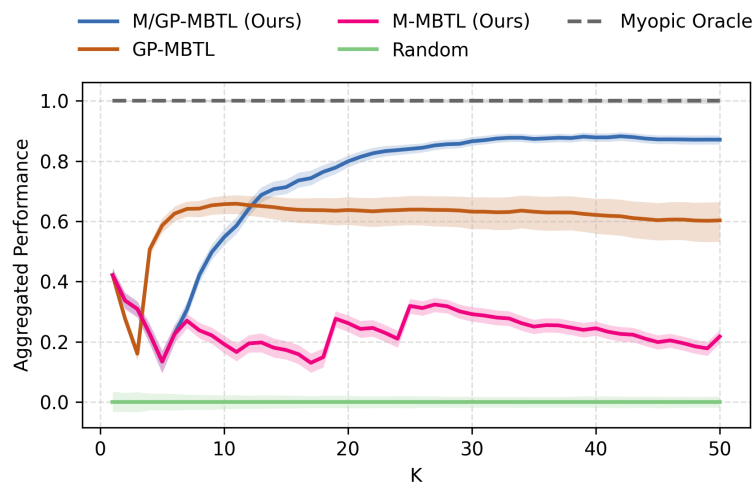


Figure 16: The plot of the aggregated metric versus (K) on the 3D synthetic dataset.

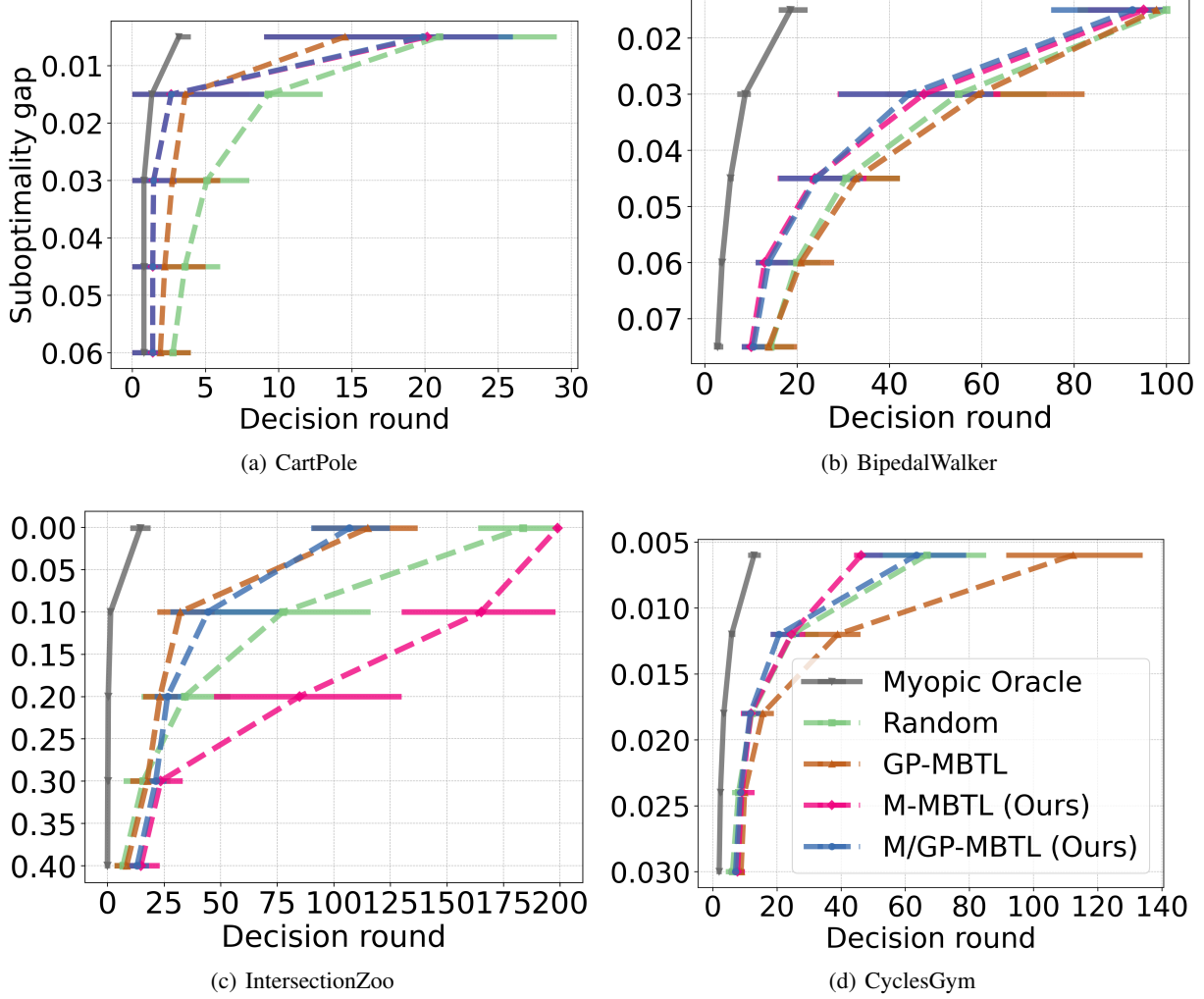


Figure 17: Number of source-trained policies required to achieve ϵ -suboptimal generalization performance in CMDP benchmarks. Lower values indicate faster convergence to near-optimal performance.

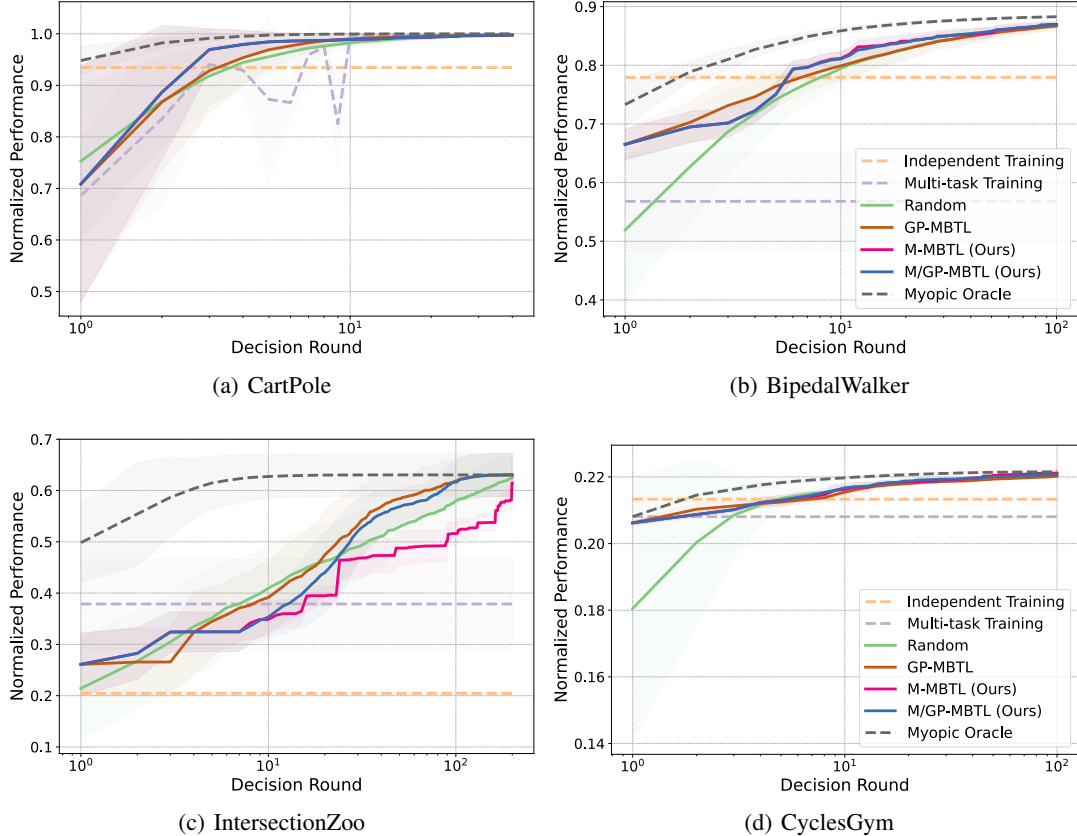


Figure 18: Normalized performance comparison of M/GP-MBTL with other baselines (Independent Training, Multi-task Training, Stochastic Oracle, Random, and MBTL baselines) on the CartPole, BipedalWalker, IntersectionZoo, and CyclesGym benchmarks.

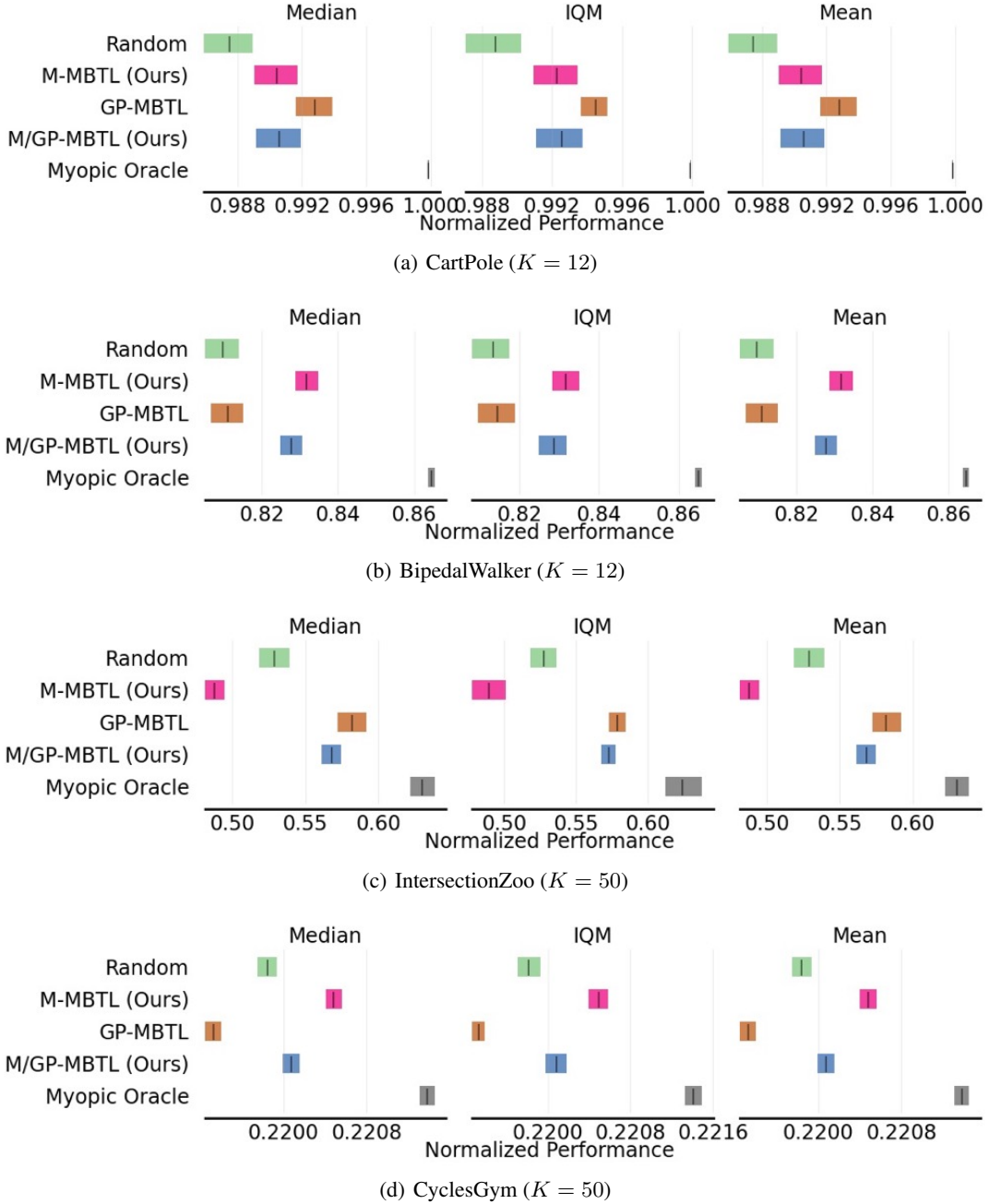


Figure 19: Performance comparison of M/GP-MBTL with baselines in terms of median, IQM, and Mean. Colored bars indicate 95% bootstrap confidence intervals for each method.

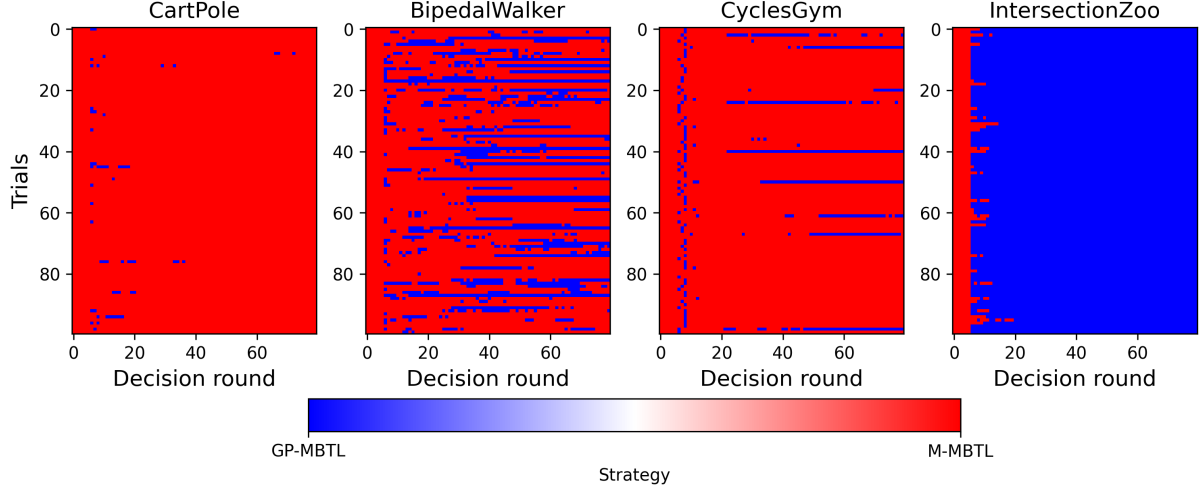


Figure 20: Per-round algorithm selection over 100 trials ($K = 80$) across four benchmarks. Red pixels indicate rounds where M-MBTL was chosen; blue where GP-MBTL was chosen. CartPole and CyclesGym remain almost entirely in M-MBTL (mountain structure), IntersectionZoo almost entirely in GP-MBTL (non-mountain), and BipedalWalker exhibits a dynamic mix.

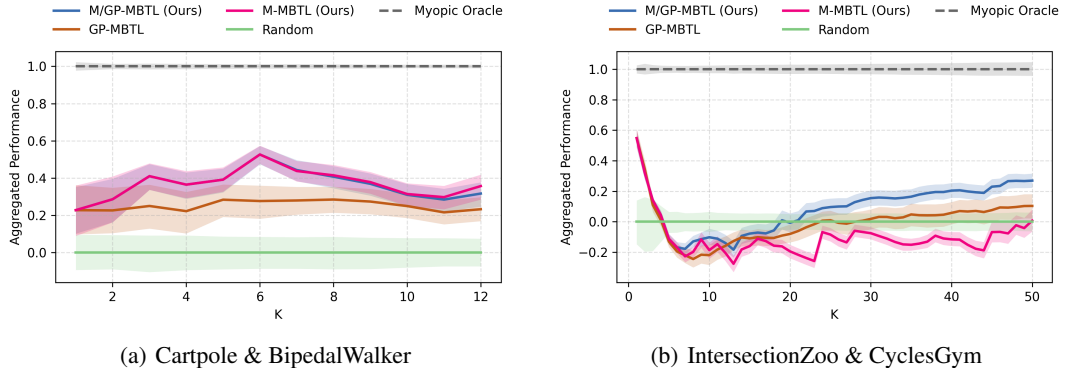


Figure 21: The plot of the aggregated metric versus K on the benchmark dataset.

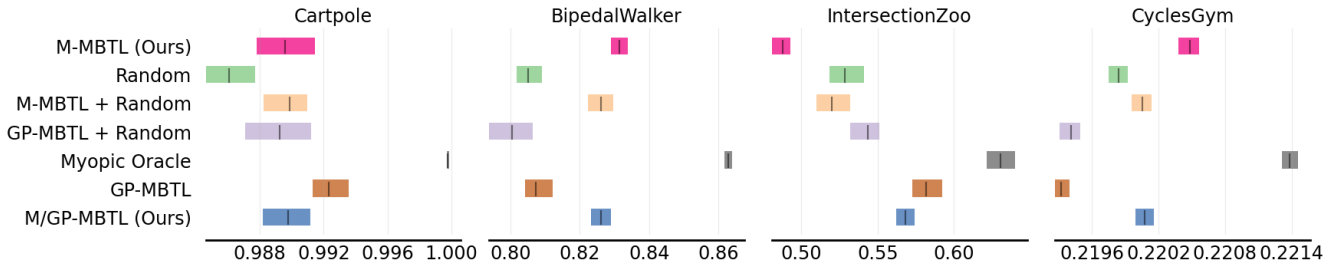


Figure 22: Ablation study comparing M/GP-MBTL with four variants—stand-alone M-MBTL, GP-MBTL, M-MBTL+Random, and GP-MBTL+Random. Colored bars indicate 95% bootstrap confidence intervals for each method.

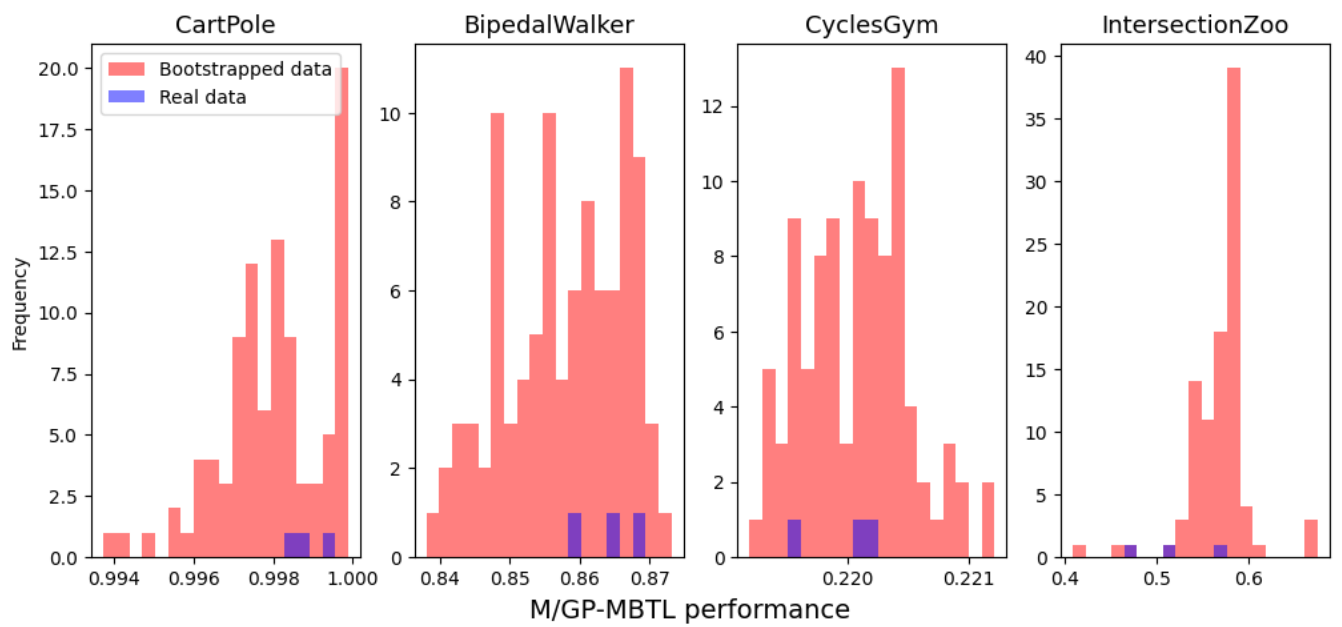


Figure 23: Histogram of M/GP-MBTL performance for real data and bootstrapped data

Reproducibility Checklist

Instructions for Authors:

This document outlines key aspects for assessing reproducibility. Please provide your input by editing this `.tex` file directly.

For each question (that applies), replace the “Type your response here” text with your answer.

Example: If a question appears as

```
\question{Proofs of all novel claims  
are included} {(yes/partial/no)}  
Type your response here
```

you would change it to:

```
\question{Proofs of all novel claims  
are included} {(yes/partial/no)}  
yes
```

Please make sure to:

- Replace ONLY the “Type your response here” text and nothing else.
- Use one of the options listed for that question (e.g., **yes**, **no**, **partial**, or **NA**).
- **Not** modify any other part of the `\question` command or any other lines in this document.

You can `\input` this `.tex` file right before `\end{document}` of your main file or compile it as a stand-alone document. Check the instructions on your conference’s website to see if you will be asked to provide this checklist with your paper or separately.

1. General Paper Structure

- 1.1. Includes a conceptual outline and/or pseudocode description of AI methods introduced (yes/partial/no/NA) **yes**
- 1.2. Clearly delineates statements that are opinions, hypothesis, and speculation from objective facts and results (yes/no) **yes**
- 1.3. Provides well-marked pedagogical references for less-familiar readers to gain background necessary to replicate the paper (yes/no) **yes**

2. Theoretical Contributions

- 2.1. Does this paper make theoretical contributions? (yes/no) **yes**
- If yes, please address the following points:
- 2.2. All assumptions and restrictions are stated clearly and formally (yes/partial/no) **yes**
- 2.3. All novel claims are stated formally (e.g., in theorem statements) (yes/partial/no) **yes**

- 2.4. Proofs of all novel claims are included (yes/partial/no) **yes**
- 2.5. Proof sketches or intuitions are given for complex and/or novel results (yes/partial/no) **yes**
- 2.6. Appropriate citations to theoretical tools used are given (yes/partial/no) **yes**
- 2.7. All theoretical claims are demonstrated empirically to hold (yes/partial/no/NA) **yes**
- 2.8. All experimental code used to eliminate or disprove claims is included (yes/no/NA) **yes**

3. Dataset Usage

- 3.1. Does this paper rely on one or more datasets? (yes/no) **no**

If yes, please address the following points:

- 3.2. A motivation is given for why the experiments are conducted on the selected datasets (yes/partial/no/NA) **NA**
- 3.3. All novel datasets introduced in this paper are included in a data appendix (yes/partial/no/NA) **NA**
- 3.4. All novel datasets introduced in this paper will be made publicly available upon publication of the paper with a license that allows free usage for research purposes (yes/partial/no/NA) **NA**
- 3.5. All datasets drawn from the existing literature (potentially including authors’ own previously published work) are accompanied by appropriate citations (yes/no/NA) **NA**
- 3.6. All datasets drawn from the existing literature (potentially including authors’ own previously published work) are publicly available (yes/partial/no/NA) **NA**
- 3.7. All datasets that are not publicly available are described in detail, with explanation why publicly available alternatives are not scientificallyatisficing (yes/partial/no/NA) **NA**

4. Computational Experiments

- 4.1. Does this paper include computational experiments? (yes/no) **yes**

If yes, please address the following points:

- 4.2. This paper states the number and range of values tried per (hyper-) parameter during development of the paper, along with the criterion used for selecting the final parameter setting (yes/partial/no/NA) **yes**
- 4.3. Any code required for pre-processing data is included in the appendix (yes/partial/no) **yes**
- 4.4. All source code required for conducting and analyz-

ing the experiments is included in a code appendix
(yes/partial/no) [yes](#)

- 4.5. All source code required for conducting and analyzing the experiments will be made publicly available upon publication of the paper with a license that allows free usage for research purposes (yes/partial/no)
[yes](#)
- 4.6. All source code implementing new methods have comments detailing the implementation, with references to the paper where each step comes from (yes/partial/no) [yes](#)
- 4.7. If an algorithm depends on randomness, then the method used for setting seeds is described in a way sufficient to allow replication of results (yes/partial/no/NA) [yes](#)
- 4.8. This paper specifies the computing infrastructure used for running experiments (hardware and software), including GPU/CPU models; amount of memory; operating system; names and versions of relevant software libraries and frameworks (yes/partial/no) [yes](#)
- 4.9. This paper formally describes evaluation metrics used and explains the motivation for choosing these metrics (yes/partial/no) [yes](#)
- 4.10. This paper states the number of algorithm runs used to compute each reported result (yes/no) [yes](#)
- 4.11. Analysis of experiments goes beyond single-dimensional summaries of performance (e.g., average; median) to include measures of variation, confidence, or other distributional information (yes/no)
[yes](#)
- 4.12. The significance of any improvement or decrease in performance is judged using appropriate statistical tests (e.g., Wilcoxon signed-rank) (yes/partial/no) [yes](#)
- 4.13. This paper lists all final (hyper-)parameters used for each model/algorithm in the paper's experiments (yes/partial/no/NA) [yes](#)

Potential impacts

Our approach could substantially lower the computational resources required to address complex, real-world CMDP problems. Although we have not identified any immediate negative societal consequences, we will continue to investigate the broader effects of deploying the methods introduced in this paper.